Spring 5-10-2019

Nanomedicine-based Immunochemotherapy for the MR Imaging and Treatment of Triple Negative Breast Cancer

Saloni Darji
Pittsburg State University, sdarji@gus.pittstate.edu

NANOMEDICINE-BASED IMMUNOCHEMOTHERAPY FOR THE MR IMAGING AND TREATMENT OF TRIPLE NEGATIVE BREAST CANCER

A thesis submitted to the Graduate School
In Partial Fulfillment of the Requirements
For the Degree of
Master of Science in Polymer Chemistry

Saloni Darji

Pittsburg State University

Pittsburg, Kansas

April 2019

NANOMEDICINE-BASED IMMUNOCHEMOTHERAPY FOR THE MR IMAGING AND TREATMENT OF TRIPLE NEGATIVE BREAST CANCER

Saloni Darji

APPROVED:

Thesis Advisor _____
Dr. Santimukul Santra, Department of Chemistry

Committee Member _____
Dr. Irene Zegar, Department of Chemistry

Committee Member _____
Dr. Dilip Paul, Department of Chemistry

Committee Member _____
Dr. Phillip Harries, Department of Biology

ACKNOWLEDGMENTS

I would like to express my special thanks to my advisor and mentor in my thesis Dr. Santimukul Santra, who gave me the opportunity to work in his lab. This work would not have been possible without his encouragement and advice.

I am very grateful to all family members for believing in me and supporting me through everything. This wouldn't have been possible without them. I also want to thank my best friend Nayan, for always encouraging me and having my back no matter what. I also want to thank all my friends back home for always believing in my abilities and uplifting me.

I am really appreciative of all my lab members for being such wonderful companions through my time in Pittsburg State University. They were always helpful and co-operative. I would also like to thank the Polymer Chemistry department for giving me this wonderful opportunity to conduct research.

NANOMEDICINE-BASED IMMUNOCHEMOTHERAPY FOR THE MR IMAGING AND TREATMENT OF TRIPLE NEGATIVE BREAST CANCER

An Abstract of the Thesis by
Saloni Darji

Breast cancers accounts for approximately 41,760 deaths every year. In women Triple negative breast cancer (TNBC) is known to be a very aggressive type of tumor. Current treatment approaches like chemotherapy and radiation therapy are abortive and have many side effects. With the recent advances in nanotechnology and immunotherapy for cancer treatment, we have designed a new nanomedicine that combines both aspects together in one cancer treatment. In this work, we have developed an anti-programmed death ligand -1 (PD-L1) conjugated, doxorubicin and gadolinium-DTPA linked (Doxo-SS-Gd) prodrug encapsulated iron oxide nanoparticles (IONPs) to form IONP-Doxo-SS-Gd-PD-L1 nanomedicine for the targeted MR imaging and treatment of TNBC. The anti PD-L1 acts as a checkpoint inhibitor in the (programmed death-1) PD-1 & PD-L1 interaction, helping generate an immune response against cancer cells. Furthermore, the gadolinium-diethylenetyramine pentaacetic acid (Gd-DTPA) functionalized doxorubicin prodrug (Doxo-SS-Gd), is known as a chemotherapeutic drug and a strong T1 MR agent, which would provide bright T1 MR contrast for the imaging of tumor. To assess the therapeutic potential of the designed nanomedicine in treating cancer, various cell based experiments were carried out. The bright and dark magnetic resonance (MR) contrast of the IONP-Doxo-SS-Gd-PD-L1 nanomedicine was also evaluated using clinical MRI instrument (B = 9.3T). Therefore, the developed immunochemotherapeutic-nanomedicine provides combination approaches for the synergistic (immunotherapy and chemotherapy) treatment

of TNBC and further has MR imaging functionality for diagnosis and treatment monitoring.

TABLE OF CONTENTS

LIST OF SCHEMES

SCHEME **PAGE**

LIST OF FIGURES

PAGE

Chapter I

Chapter II

LIST OF ABBREVIATIONS

IONPs: Iron oxide nanoparticles

PAA: Poly (acrylic acid)

Doxo: Doxorubicin

Gd-DTPA: Gadolinium diethylenetyramine pentaacetic acid

ICAM-1: Intracellular adhesion molecule-1

PD-L1: Programmed death ligand 1

PD-1: Programmed death 1

TNBC: Triple negative breast cancer

DSP: Dithiobis(succinimidyl propionate)

IONP-COOH: Carboxylated iron oxide nanoparticles

IONP-ICAM-1: Intracellular adhesion molecule-1 coated iron oxide nanoparticle

IONP-PD-L1: Programmed death ligand-1 coated Iron oxide nanoparticle

EDC: 1-ethyl-3-(3-dimethylaminopropyl) carbodiimide)

NHS: N-hydroxy succinimide

DMSO: Dimethyl sulfoxide

PHA: Polyheamagglutinin

MTT: (3-(4, 5-dimethyl-thiazol-2-yl)-2, 5 diphenyl tetrazolium bromide)

PBS: Phosphate buffer saline

DAPI: 4′,6-diamidino-2-phenylindole

IL-2: Interleukin 2

MALDI-TOF: Matrix-assisted laser desorption/ionization- time of flight

MRI: Magnetic resonance imaging

DLS: Dynamic light scattering

Chapter I

Introduction:

Nanoscience has played a vital role in revolutionizing the field of science and technology. With advances in research and development, nanotechnology has gained tremendous momentum in the pharmaceutical industry, which mainly embraces development of nanodevices, nanoformulations and nanomaterials (1). Over the last two decades, nanotechnology has been looked upon as a promising platform for treatment of various kinds of cancer using nanocarriers for drug delivery (2). Conventional treatment methods like surgery, radiation, and chemotherapy are still practiced in clinical setting but may have undesirable implications. Surgery is important for the removal of tumor, but it cannot eradicate the cancerous cells which have metastasized. Chemotherapy and radiotherapy have their own negative effects like, damage to healthy cells, severe nausea, drug resistance, and damage to the immune system (3). Nanotechnology is a very efficient system to overcome these limitations due to its unique properties. The ability to achieve targetability, greater biocompatibility, reduce toxicity, and multi-functionality makes it ideal for using as a therapeutic drug delivery system (4). There are many different forms of nanosystem like, lipid-based nanoparticles, polymeric nano constructs, silica nanoparticles, silver nitrate nanoparticles, cerium oxide nanoparticles, gold based

nanosystem, and iron oxide nanoparticles which are currently used for development of novel therapeutics for drug delivery (5).

1) Nanomaterial based Chemotherapeutic treatment

1.1) Polymeric Nano constructs:

Various types of polymer-based nanoparticles have been developed for the treatment of cancer. Amongst all, dendrimers are a class of polymer that withholds unique properties, ideal for acting as a drug carrier. The well-defined structure, uniformity, modifiable nanosize, and abundant surface functional groups allow researchers to tune the dendrimer for specific applications (6,7). With various kinds of dendrimers available, polyamidoamine (PAMAM) dendrimers have been widely used for therapeutic purposes (8). Pan et. al., demonstrated the use of PAMAM copolymer with polyethylene glycol (PEG), as drug delivery vehicle for the treatment of multidrug resistant (MDR) ovarian and breast cancers. The co-polymeric system was loaded with doxorubicin and therapeutic siRNA, and the cytotoxicity of this nanosystem was evaluated for ovarian and breast cancer, demonstrating the increased cytotoxicity and decreased drug resistance due the polymeric nanosystem (9). The symmetrical structure of dendrimer allows it to function like small molecules, however, it is relatively difficult to synthesize a perfect dendrimer. Hyperbranched polymers on the other hand are feasible to synthesize, therefore being looked as an alternative approach for drug delivery (10). Santra et al. demonstrated multifunctional hyperbranched polyester (HBPE) which were used for targeting and killing cancer cells. The HBPE core was loaded with therapeutic drug Taxol for the curative effect, DiI dye and MR contrast agent for the detection purpose. Furthermore, the surface of HBPE

was modified to folate to give the nanocarrier targetability. This nanosystem was successfully tested in lung cancer and cervical cancer cells, proving its potential to effectively target and treat cells in addition to the MR imaging (11).

1.2) Lipid-based nanocarrier:

Liposomes are one of the most established nanocarriers used in the field of drug delivery. Lipid vesicles mimic the function of normal phospholipid bilayer membrane of the cells, allowing the easy internalization into the targeted cells. Liposomes have excellent biocompatibility, biodegradability, and ability to hold hydrophilic & hydrophobic cargos (**Figure 1**). The wide range of physicochemical properties makes it appropriate for drug delivery system (12,13).

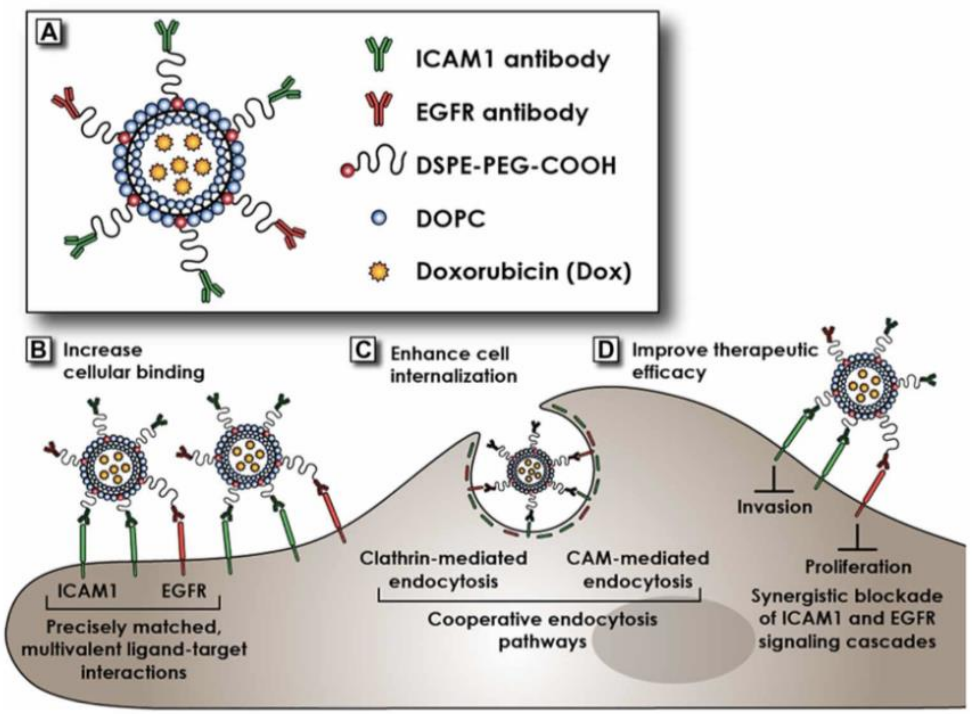

Figure 1: Schematic representation of dual complementary liposomes targeting TNBC cells via two different targeting liposomes.

Doxil, a liposomal formulation of Doxorubicin has been approved by the FDA for treating cancer in AIDS related sarcomas. With the firm establishment of liposomes, scientists continue to investigate different models intending to improve chemotherapy outcomes (14). In a recent study, dual complementary liposomes (DCL) were developed by coating with intracellular adhesion molecule-1 (ICAM1) and epithelial growth factor receptors EGFR, for targeting Triple negative breast cancer cells (TNBC). These DCLs were incorporated with doxorubicin in the cargos. When the DCL system was tested against the TNBC tumor cells, the results indicated an increase in binding and internalization because of the multivalent ligand on the surface as compared to the single targeting ligand. Furthermore, there was a substantial decrease in the tumor volume due to the multivalent binding, proving the potential of DCLs in curing TNBC tumor (15).

1.3) Gold and Silver nanoparticles:

The discovery of ruby gold nanoparticles was done by Michael Faraday in 1857 served as the foundation of modern nanotechnology (16). Since then many scientists have studied the preparation process and the properties of gold nanoparticles (17-19). With the use of modern technology, the applications of gold nanoparticles (AuNPs) have broadened. The excellent optical, physical, and chemical properties of AuNPs when harnessed with a proper approach, opens an immense ranged of applications from tagging, imaging and sensing to biomedical diagnosis, detection and drug delivery. In the past few years, the AuNPs have been widely used in the biomedical field for imaging and therapeutics. The unique optical, photothermal, binding properties with various organic and biological organisms, reduced toxicity, controlled drug release and strong absorption spectrum make

AuNPs suitable for acting as a carrier for various therapeutics (20). Various models of AuNPs have been proposed and used in studies for the treatment of cancer cells (21-22).

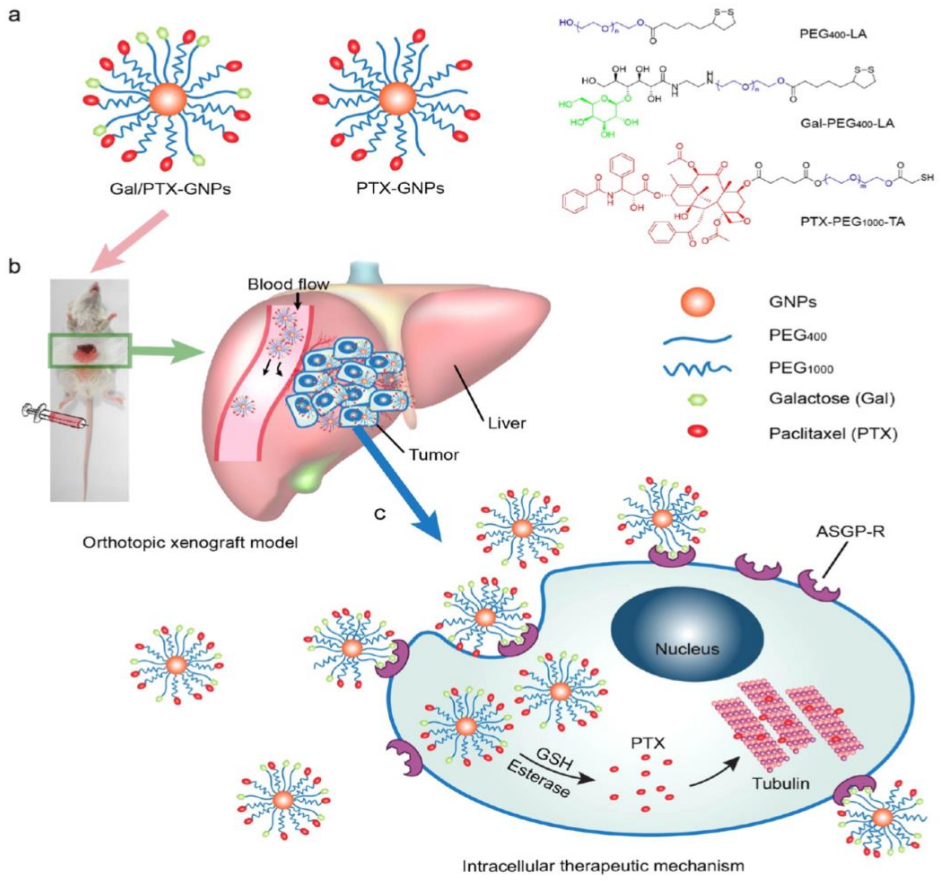

Figure 2: (A) schematic diagram of Gal/PTX-GNPs (B) Endocytosis scheme of galactose coated gold nanoparticles, selectively targeting liver carcinoma for paclitaxel drug delivering.

Gao et. al., introduced a novel method for intra-organ targeting of liver cancer using gold nanoparticles (GNPs, **Figure 2**). In this model, GNPs were conjugated with galactose for targeting the asialoglycoprotein receptor (ASGP-R) of the liver carcinoma, and paclitaxel was loaded in GNPs for therapeutic effect. The specific targeting ability contributed to the reduction in hepatotoxicity and improved the antitumor activity in the liver carcinoma

treatment. Overall this model allowed selective targeting of liver carcinoma and improve the treatment of both heterotopic and orthotropic liver tumors (23). In addition to gold nanoparticles, silver nanoparticles are also well known for their antimicrobial and anticancer properties. Furthermore, their surface plasmon resonance, easy surface charge modifications and shape reformation, make them a good fit for using in targeted drug delivery for cancer treatment. Hence, various studies have been done to test their potential in cancer treatment (24).

1.4) *Iron oxide nanoparticles:*

Magnetic nanoparticles or iron oxide nanoparticles (IONP) are a class of inorganic nanoplatforms used for imaging, detection, and treatment of cancer. The following distinct characteristic of IONPs makes them suitable as drug delivery systems: 1) excellent biocompatibility and bio-distribution, 2) strong magnetic properties, 3) alterable surface functional groups, and 4) high drug load retention capacity. Therefore, iron oxide nanoparticles have vast biomedical applications ranging from MR imaging, hyperthermia, bio nanosensors, and targeted drug delivery system (25,26). Several studies have tested IONPs as targeted drug delivery and imaging system for cancer (27,28).

Recent investigations proposed the use of IONPs for treating drug resistant ovarian cancer (29). To achieve the targetability, optical imaging and therapeutic properties, the surface of IONP was conjugated with NIR-830 dye labelled HER2 antibody, and further loaded with cisplatin. (**Figure 3**) The unique MR and optical imaging of this system helped in examining the targeted drug delivery system, especially in tumors with overexpressed heterogeneous HER-2 expressing and further determine the intra-tumoral distribution of

nanoparticles. This study demonstrates the effective treatment of HER-2 overexpressed and drug resistant ovarian cancer (29).

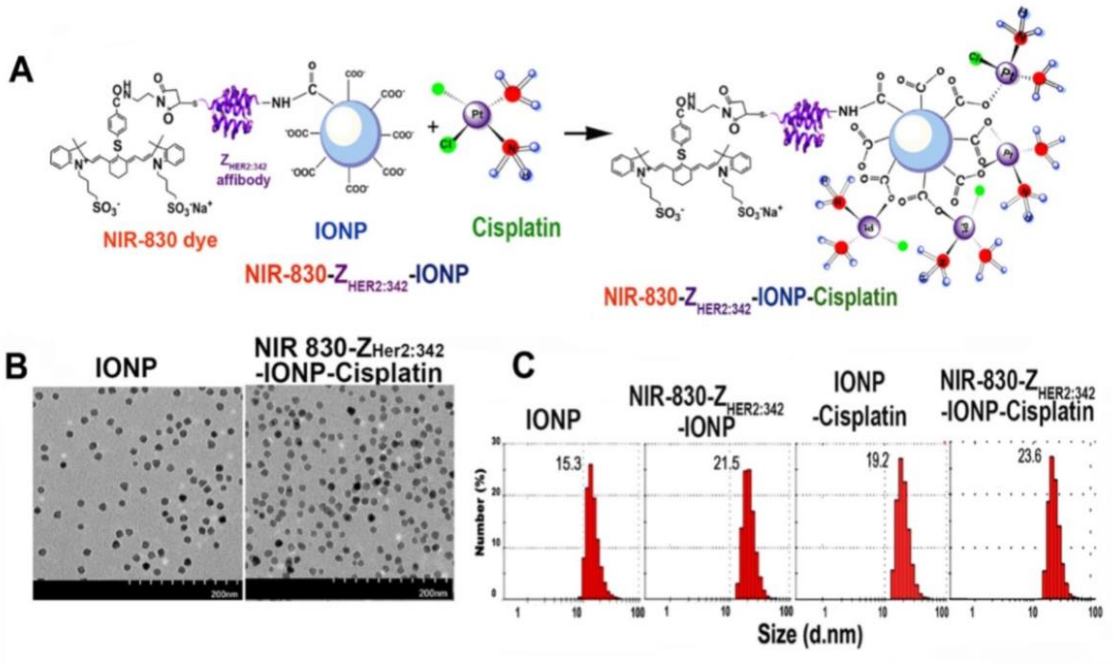

Figure 3. (A) Schematic diagram of synthesis scheme of NIR-830-$_{ZHER-324}$-IONP and (B) TEM images of different nonoperation's, (C) Zeta potential of different Nano preparation (29).

2) Molecular immunotherapy

The promising research conducted on the role of nanoparticles as potential drug delivery systems in cancer treatment, led to their entry into the clinical trial stage. Some lipid-based nanoparticles (Doxil, doxisome, daunoxome), albumin nanoparticles (Abraxane), and polymeric nanoparticles (Oncaspar, Zinostatin stimalamer) are some examples that underwent clinical trials.

Most of the nano-models have been designed to directly act on the tumor, overlooking the crucial role of immune system in the development, proliferation, and

resolution of cancer. Studies have also suggested a strong correlation between immunosuppressive cells and the tumor cells. As a result, 2013 was reported as “cancer immunotherapy” breakthrough year. Since then, researchers have tried to study the role of immune system in cancer and further introduced different types of immunotherapeutic treatments for various kinds of cancer (30,31). There are several kinds of cancer immunotherapeutic approaches which have proven to have excellent clinical responses. Following are the main categories of immunotherapy treatment include, 1) T-cell transfer especially the chimeric antigen receptor T (CAR-T) cell therapy 2) Cytokine therapy and 3) Checkpoint blockade therapy (32).

2.1) CAR-T cell therapy:

CAR-T therapy involves the use of genetically engineered T cells for expressing chimeric antigen receptor, which can be particularly directed towards an antigen on a patient’s tumor cells. This would successfully target and eradicate cancer cells with the help of immune cells. The T cells can either be derived from patients’ blood or a healthy donor (33). As CAR-T cells attack the cancer cells they also recruit more immune cells by releasing cytokines and killing the cancer cells. In 2010, a study conducted using CD19 CAR T cells for treating a patient with lymphoma had very promising outcomes. Since then, CAR T cell therapy have had amazing effects in treating patients with a relapse of acute or chronic leukemia (34). A very recent breakthrough in the field of CAR-T treatment was when the U.S. Food and Drug Administration (FDA) approved Kymriah, a cell therapy for treatment. Kymriah is genetically engineered by using one’s own immune cells to attack a type of leukemia. Not long after that, Yescarta, a kind of CAR-T cell therapy was

approved by FDA. Unlike the conventional methods, in these type of medicine a unique model is developed from the T cells of patients for the treatment. While currently these therapies are only available for treatment of very rare types of blood cancer, efforts have been made to develop CAR-T therapy for solid tumors. This must include targeted engineering and more robust system, as there is a fine line between killing cancer cells and killing the healthy cells. Although CAR-T therapy has its own pros and cons, it brought a revolutionary change in the field of cancer immunotherapy and upsurged the hope of patients suffering from the disease (35).

2.2) Cytokine therapy:

Cytokines are messengers secreted by innate and adaptive immune cells, in response to the presence of antigens. There are two main types for cytokines, 1) interleukins and 2) interferons. These messengers allow the immune system to communicate and generate a robust immune response for targeting the antigen. Immune effector and stromal cells are stimulated by cytokines at the tumor site and hence, cell recognition by cytotoxic effector cells is enhanced. There are series of common receptors which play a role in signaling. Until now, seven classes of cytokine receptors who help in conducting the signals are identified. Various studies have been performed to test the anti-tumor activity of cytokines. Several cytokines like, GM-CSF, IL-1, IL-2, IL-7, IL-12, IL-15, IL-18 and IL-21 entered clinical trials for patients with advance cancers. Furthermore, IL-2 has been approved by FDA for the treatment of metastatic melanoma and renal carcinoma and INF-alpha has been approved for treating stage III melanoma. The potential of cytotoxic therapy's potential in cancer immunotherapy can be best demonstrated by IL-2 treatment, which can induce amazing response in the renal carcinoma and metastatic

melanoma patients (36,37).

2.3) Checkpoint blockade therapy:

The capability of the immune system to distinguish between normal and carcinoma cells is the basis for immunotherapy treatment. Cancer cells have various mechanisms to avoid immune mediated rejection. They either lose or decrease their antigenicity by mutation. For example, INF-γ produced by tumor infiltrating lymphocytes induces the overexpression of programmed cell death ligand-1 (PD-L1) on tumor cells. Inhibitory checkpoint or checkpoint blockade downregulates the antitumor immunity, by acting on the immunogenic checkpoint proteins. These checkpoint proteins can be of two kinds: i) stimulatory checkpoint proteins like TNF-alpha, CD40 and CD27 and ii) inhibitory checkpoints, which includes PD-1, CTLA-4 and LAG3. Inhibitory checkpoints are common targets for checkpoint blockade therapy. Programmed cell death 1 (PD-L1) are proteins found on T-cells and B-cells. Since many cancer cells have PD-L1 expressed on the surface, this ligand tends to interact with the PD-1 of immune cells to escape T-cell mediated immune response. Therefore, blocking the interaction between PD-1 and PD-L1 would help in recruiting T cells for killing cancer. The interaction could be broken either by using anti-PD-L1 or anti-PD-1 blockade. This therapy has been tested on various PD-L1 overexpressing tumors like glioblastomas, lymphoma and lung cancer. Furthermore, Pembrolizumab and Nivolumab are the first anti-PD-1 checkpoint inhibitor approved by FDA. (**Figure 4**) Both the checkpoint inhibitors have shown promising result in phase I/II trails, moving them to phase III. Hence, checkpoint blockade holds potential to be in the clinical setting for curing cancer (39-41).

Immune checkpoint modulators in clinical trials

Target	Drug	Source	Clinical testing phase
PD-1	PDR001	Novartis	Phase I/II
	Pidilizumab	Medivation	Phase II
	JS001	Shanghai Junshi Bioscience	Phase I/II
	SHR-1210	Incyte	Phase I/II
	TSR-042	Tesaro	PhaseI
PD-L1	KN035	3D Medicines	Phase I
GITR	TRX518	Leap Therapeutics	Pahse I
	MEDI1873	MedImmune	Phase I
	BMS-986156	Bristol-Myers Squibb	Phase I
	MEDI16469	MedImmune	Phase I
LAG-3	LAG525	Novartis	Phase I
	BMS-986016	Bristol-Myers Squibb	Phase I
	IMP321	Prima BioMed	Phase I
TIM-3	MGB453	Novartis	Phase I/II
	MEDI19447	MedImmune	Phase I

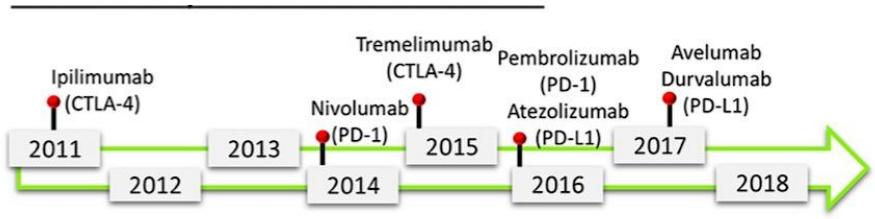

Figure 4. List of immune checkpoint modulators, which are in clinical trials and series of modulators already in clinic (38).

Cancer can affect any organ of human body. A lot of research is being done to better understand the mechanisms of the cancer, which could help in coming up with a better cure. In cancer, every other case is unique from the previous one, making it difficult for the scientists to establish a perfect generalized treatment method without any ill effects for the cancer patients. Several different types of treatment approaches, ranging from simple radiation therapy to more complex immunotherapy have been studied and practiced

for curing cancer. Therefore, scientists from all around the globe further continue to investigate complexities relating to cancer hoping to find a better solution in order to overcome the drawbacks of current treatment methods. In this study, we combined chemo- and immunotherapies for the treatment of TNBC using modern nanotechnology as a targeted delivery system.

Chapter II

Introduction

In this study, we have designed a nanomedicine for targeted treatment and MR imaging of the TNBCs. The lack of three main hormonal receptors: estrogen receptor (ER), progesterone receptor (PR) and, human epidermal growth receptor 2 (HER-2) makes it triple negative. This nanomedicine has a dual treatment action for cancer, combining immunotherapy and chemotherapy. PD-1/PD-L1 checkpoint inhibition is a widespread immunotherapeutic technique for treating numerous tumors. MDA-MB-231, a type of TNBC which overexpress PD-L1 ligand on the surface which, binds to the PD-1 ligand on the T-cells. This interaction suppresses the antitumor activity of T cells by mechanisms, by decreased cytokine production and inhibiting the cytotoxic-T cells response. However, obstructing this response results in triggering the immune cells to recognize cancer as foreign and leading to its destruction. We developed anti-PD-L1 Ab conjugated iron oxide nanoparticles (IONPs), which we hypothesized will help in targeting MDA-MB-231 and most importantly, break the PD-L1/PD-L1 interaction to generate a strong immune response (**Figure 1**). Furthermore, to incorporate chemotherapeutic and imaging capability, we encapsulated a prodrug within the PAA coatings of IONPs. This prodrug has two main components: 1) Doxorubicin (Doxo), which acts as a chemotherapeutic agent for killing the cancer cells and 2) Gadolinium complex (Gd-DTPA), which is responsible

for the T1-based bright contrast in the MR imaging of the tumor. These two components were linked via a disulfide linker dithiobis(succinimidyl propionate) (DSP), to form Doxo-SS-Gd. All these components were assembled to form IONP-Doxo-SS-Gd-PD-L1 nanomedicine.

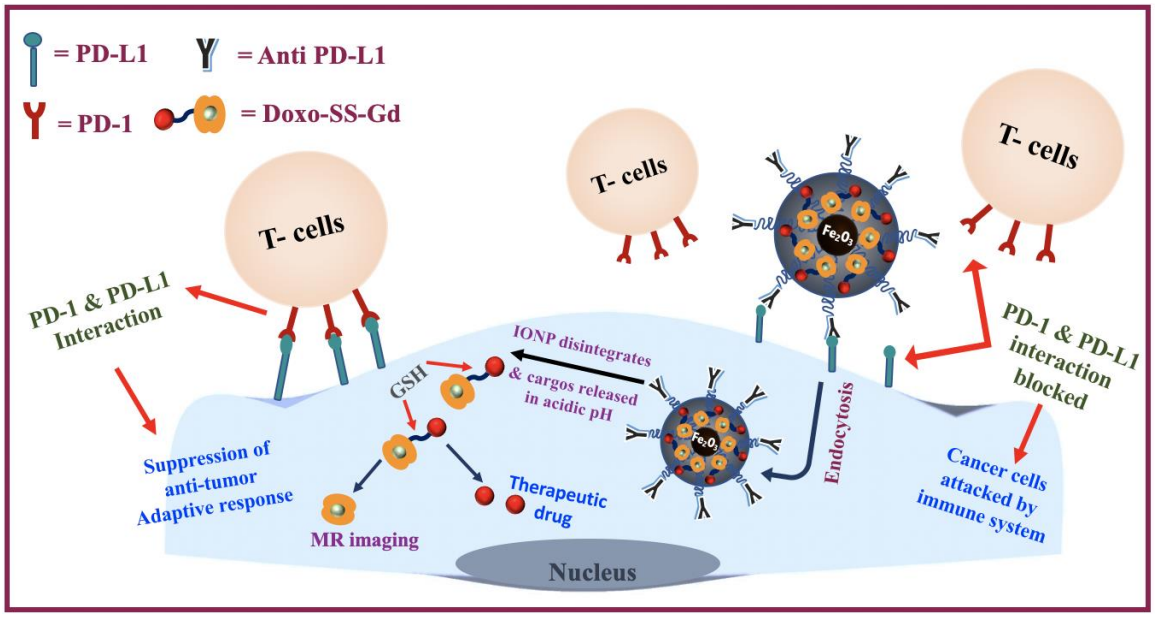

Figure 1: Schematic representation of the events taking place in the system when in presence and absence of IONP-Doxo-SS-Gd-PD-L1.

The synthesized nanomedicine, helps in breaking the PD-1 & PD-L1 interaction, facilitating the targeted internalization into the tumor with the help of anti PD-L1 on the IONP-Doxo-SS-Gd-PD-L1. Once the nanomedicine is inside the TNBCs, IONPs swell due to the acidic micro-environment inside the cell, releasing the prodrug. When Doxo-SS-Gd is released from the nanomedicine, the T1 contrast agent Gd gets activated. Although T1 signal is active in prodrug form but therapeutically, Doxo remains inactive. Glutathione, an enzyme present in abundance inside cancer cells, cleaves the disulfide

linkage and therefore releases Doxo making it therapeutically active. Our nano-chemoimmunotherapeutics is a unique model, which holds the capability to attack tumor cells by two completely different mechanisms while allowing the monitoring of the treatment.

2) Results and discussion

2.1) Synthesis of Doxo-SS-Gd:

The synthesis of Doxo-SS-Gd prodrug (**Scheme 1**) was carried out with the help of DSP crosslinker, using a conjugation technique reported earlier (42). This probe has two main components 1) Doxorubicin or Doxo and 2) gadolinium-diethylenetyramine pentaacetic acid or Gd-DTPA (Gd) complex. Doxorubicin is known to intercalate with DNA and disrupt topoisomerase-II mediated DNA repair mechanism (43). Furthermore Gd-DTPA is typically used as a T1 contrast agent in MR bioimaging (44). The prodrug once synthesized, was purified using PD-10 column (Sephadex G-25 resin) and further encapsulated in IONPs. Once the prodrug is encapsulated into IONPs, the T1 MR signals of Gd is quenched due the presence of strong T2 MR signals from IONPs. However, when the nanosystem comprising Doxo-SS-Gd prodrug enters the cancer cells, series of events takes place which leads to activation of the Doxo and T1 MR signals.

2.2) Characterization of Doxo-SS-Gd:

The Doxo-SS-Gd prodrug was characterized by analyzing the fluorescence emission and relaxation time of Doxo and Gd respectively. As seen in **Figure 2A,** the

maximum absorbance of Doxo was found to be λ_{abs} = 490 nm and the maximum fluorescence was observed to be λ_{max}= 595 nm (**Figure 2B**).

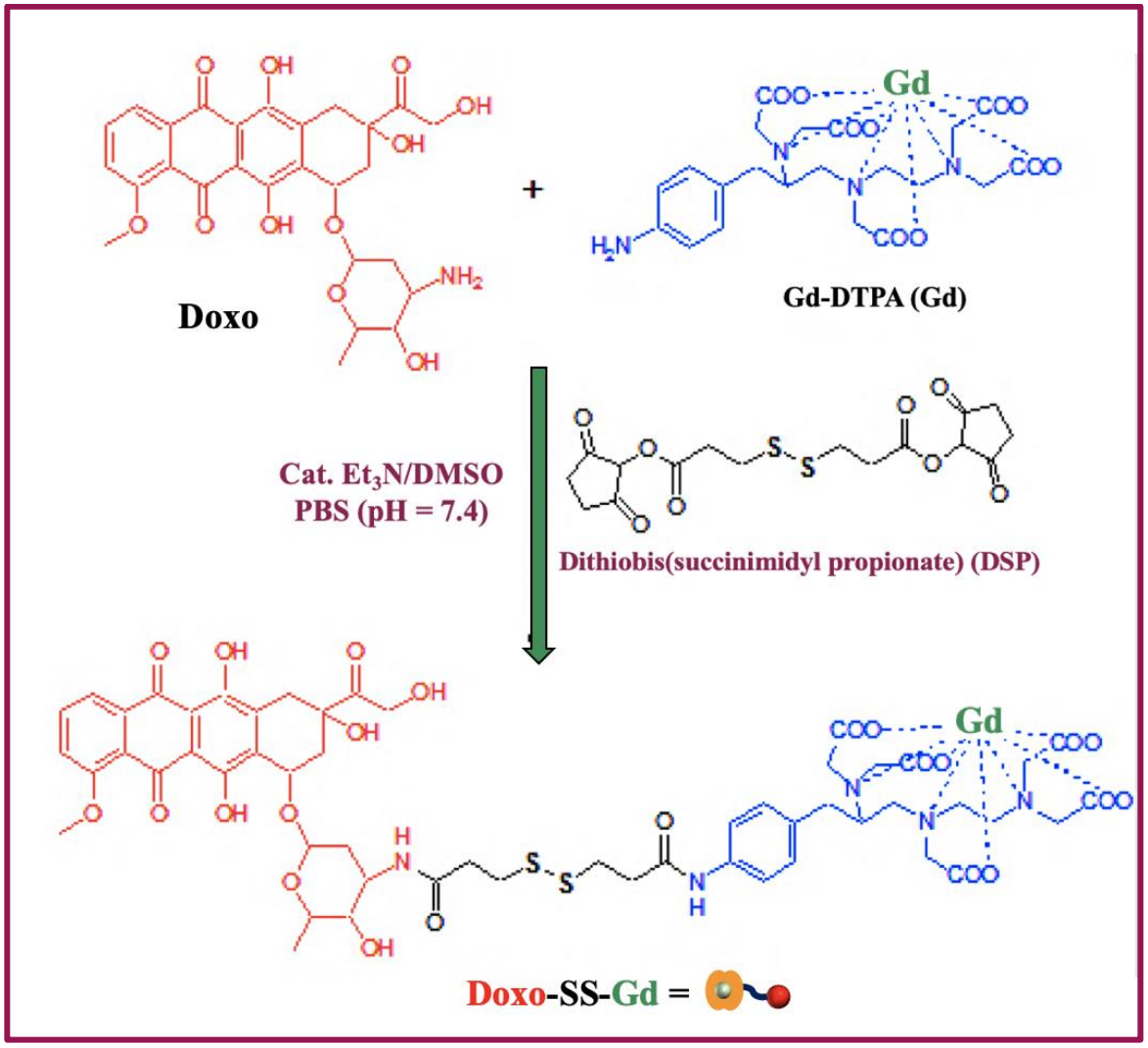

Scheme 1: Synthesis scheme of activatable Doxo-SS-Gd prodrug.

These values lie within the emission and absorbance range of Doxo indicating its presence in the prodrug. It is important to note that the doxorubicin's fluorescence

modality was not quenched since the Gd-DTPA is not a chromophore. Furthermore, the relaxation time of this prodrug was tested using benchtop MRI (B = 0.47 T). As shown in **Figure 2C,** the longitudinal relaxation time was, T1 = 85 ms (**Figure 2C**) and the transverse relaxation value measured was, T2 = 500 ms (**Figure 2D**). This indicates the signals are due to the presence of T1 active agent, Gd.

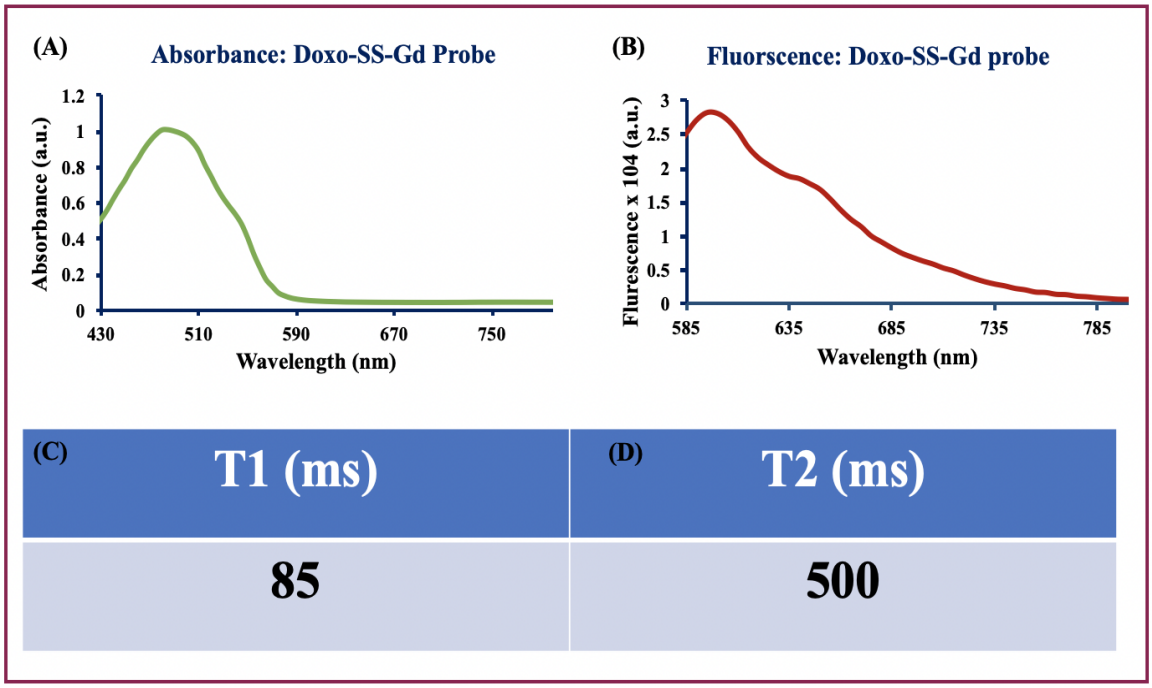

Figure 2: Characterization of Doxo-SS-Gd: (A) Absorbance intensity found to be λ_{abs} = 490 nm. (B) Fluorescence intensity measure was λ_{max}= 595 nm. (C) relaxation time T1 = 85 ms. (D) Transverse relaxation time T2 = 500 ms.

In addition to this, the synthesized Doxo-SS-Gd prodrug was also characterized using Bruker's Microflex MALDI-TOF spectrometer using dihydrobenzoic acid as matrix. A molecular ion peak at 1210 Da (M-5H) was detected, which represented the molar mass

of Doxo-SS-Gd prodrug (**Figure 3**). It further indicates that 5 protons were eliminated from DTPA during the ionization process. In addition, ICP-MS a spectrometry analysis was performed for Doxo-SS-Gd indicated the presence of Gd (0.283 mg/mL). Taken together, the characterization data indicates the successful synthesis of Doxo-SS-Gd prodrug.

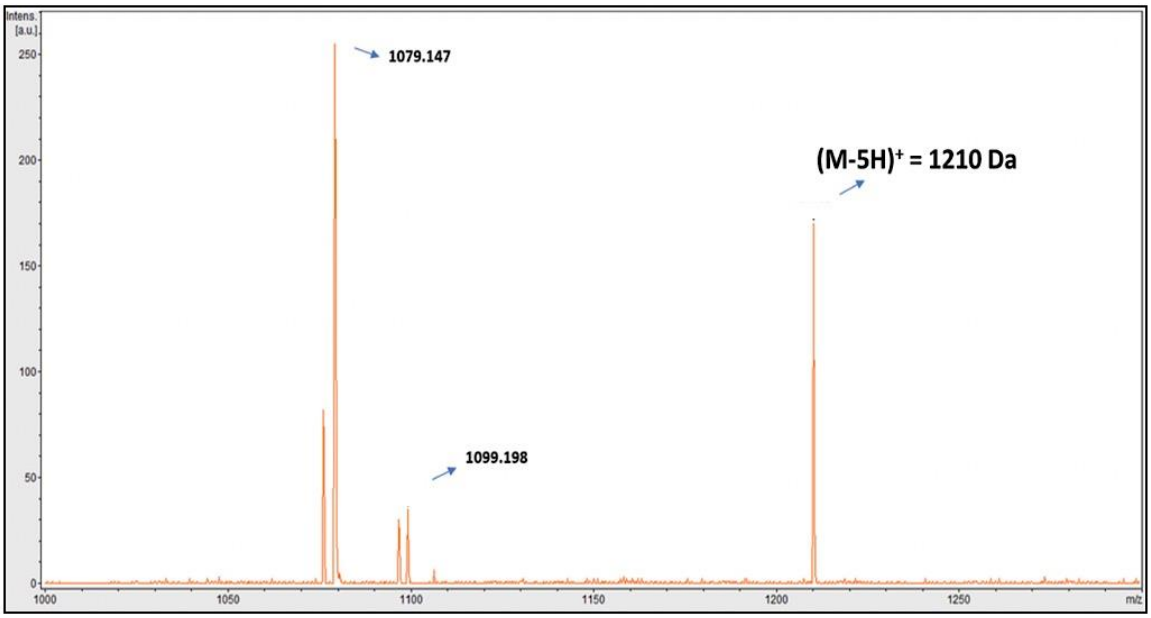

Figure 3: MALDI-TOF spectrum of Doxo-S-S-Gd-DTPA prodrug.

2.3) Synthesis and characterization of IONP-COOH:

The polyacrylic acid (PAA)-coated iron oxide nanoparticles (IONP) were synthesized using solvent precipitation method and the surface functionalization was carried out by EDC/NHS carbodiamide functionalization chemistry (**Scheme 2**).

To synthesize IONPs, $FeCl_3$ and $FeCl_2$ salts were mixed in 2:1 ratio and dissolved in an acidic solution. A basic solution (NH_4OH) and PAA solution were also

prepared prior to synthesis. PAA acts as a surface coating to the iron oxide core and, prevents the nanoparticles from aggregating. The synthesis was carried out using solvent precipitation technique where the acidic solution of iron salts was added into NH_4OH base solution, followed by the addition of PAA preparation. This mixture was allowed to react at appropriate vortexing speed at room temperature for 1 h. After the completion of the synthesis, IONP-COOH was purified by using a magnetic column and finally by dialysis against deionized water (DI) (dialysis bag MWCO = 6-8 kDa). The magnetic column helps in selectively passing unreacted nonmagnetic components and further, pure magnetic nanoparticles are obtained. Furthermore, after dialysis helps in getting rid of small unreacted components in the solution. The purified IONP-COOH (**1, Scheme 2**; [Fe] = 4 mM) was characterized by testing the size and zeta potential using dynamic light scattering. As seen in **Figure 4 C-D,** the size of IONP-COOH was found to be 65 ± 4 nm and the corresponding zeta was -24 ± 3 mV. The negative zeta potential suggests the presence of carboxylic groups on the surface of nanoparticles. After the characterization, these nanoparticles were stored at 4 °C for further use.

2.4) Anti PD-L1 functionalization on IONPs using EDC/NHS chemistry:

Anti-PD-L1 Ab is known to be a checkpoint inhibitor in PD-1 & PD-L1 interaction, and hence, is responsible for the generation of immune response. Therefore, anti PD-L1 was conjugated to test the potential of killing cancer cells using the immune system. The IONPs were conjugated by anti-PD-L1 using EDC/NHS surface chemistry to form IONP-PD-L1 (**2, Scheme 2**).

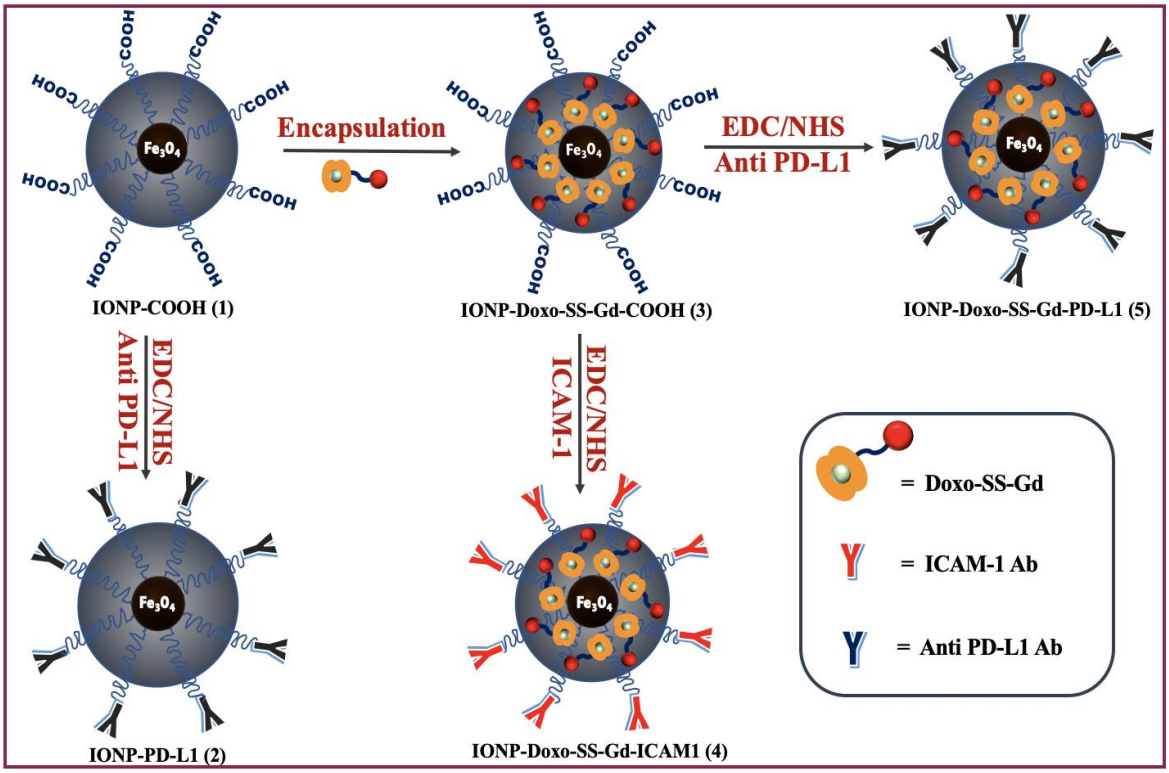

Scheme 2: Synthesis of functionalized IONP-ICAM1/IONP-PD-L1 with the help of EDC/NHS chemistry and further synthesis of IONP-Doxo-SS-Gd-ICAM1/ IONP-Doxo-SS-Gd-PD-L1 using solvent diffusion method.

Subsequently the synthesized IONP-PD-L1 particles were purified using magnetic column and dialysis as described earlier. The size and zeta potential of purified IONP-PD-L1 particles ([Fe] = 2 mM; **2, Scheme 2**) were determined to be 92 ± 6 nm and -17 ± 1 mV respectively (**Figure 4 C-D**). The increase in size is consistent with the addition of the antibody on the surface of IONP-COOH as a result of the conjugation reaction. Furthermore, the change in zeta potential is also an indication of successful conjugation.

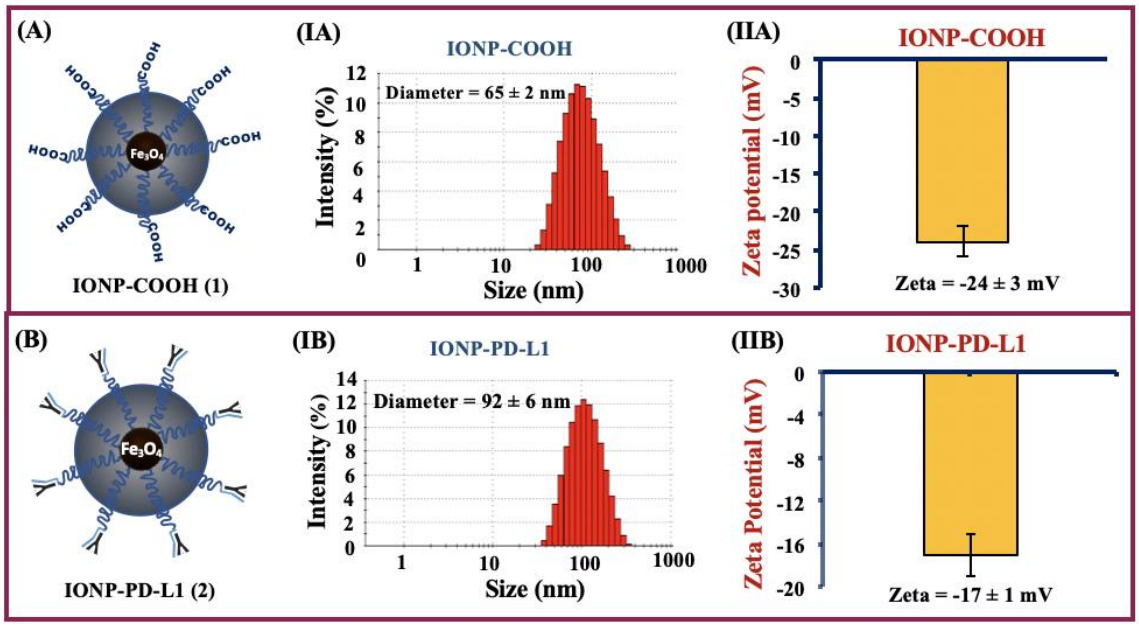

Figure 4: (A) The size and zeta potential IONP-COOH measured were (IA) 65 ± 2 nm and (IIA) -24 ± 3 mV. (B) The diameter of IONP-PD-L1 was (IB) 92 ± 6 nm and the surface zeta potential (IIB) was -17 ± 1 mV.

2.5) Encapsulation of the prodrug using the solvent diffusion method:

Doxo-SS-Gd prodrug was encapsulated into IONP-COOH using the solvent diffusion technique. A dilute solution of Doxo-SS-Gd was prepared and slowly added to IONP-COOH to obtain IONP-Doxo-SS-Gd (**3, Scheme 2**). The hydrophobicity of the prodrug drives it to go into the nanoparticles. After the synthesis, the resulting solution of IONP-Doxo-SS-Gd-COOH (**3, Scheme 2**) were purified using magnetic column and dialysis as described earlier and the final concentration of IONP-Doxo-SS-Gd-COOH found to be 2 mM.

2.6) Conjugation of anti PD-L1/ ICAM1 to IONP-Doxo-SS-Gd-COOH:

ICAM-1 and PD-L1 antibodies were conjugated to IONP-Doxo-SS-Gd-COOH to obtain the solutions of IONP-Doxo-SS-Gd-ICAM-1 (**4, Scheme 2**) and IONP-Doxo-SS-Gd-PD-L1 (**5, Scheme 2**). The conjugation was carried out using the technique previously described (EDC/NHS chemistry). Here, the ICAM-1 antibody has been used because of its overexpression in MDA-MB-231. Therefore, targeted drug delivery can be achieved to test the potential of the prodrug by itself in treating the cancer. Furthermore, anti-PD-L1 was conjugated to IONP-Doxo-SS-Gd-COOH. Due to the presence of both anti-PD-L1 and prodrug, this nanomedicine possesses dual, chemotherapeutic and immunological property and hence, can be tested for the combined treatment. After carrying out the conjugations, both the solutions were purified and characterized.

2.6.1) Characterization of IONP-Doxo-SS-Gd-ICAM1:

The solution of IONP-Doxo-SS-Gd-ICAM1 (**4, Scheme 2;** [Fe] = 1 mM) was characterized using various techniques to test the success of the conjugation of ICAM-1 and the presence of Doxo-SS-Gd prodrug. Firstly, the size and zeta potential were measured using the dynamic light scattering (DLS). The hydrodynamic diameter of IONP-Doxo-SS-Gd-ICAM1 was noted to be 85 ± 2 nm (**Figure 5 A**) and the zeta potential was -20 ± 1 mV (**Figure 5 B**). The increase in size after conjugation indicated the presence of ICAM-1 on the surface of IONP. Additionally, the change in the zeta potential from -24 ± 3 mV (IONP-COOH) to -20 ± 1 mV confirms the surface functionalization of ICAM-1. Furthermore, to test the presence of Doxo-SS-Gd, absorbance and fluorescence intensity of IONP-Doxo-SS-Gd-ICAM1 were measured. The maximum absorbance was observed at λ_{abs} = 490

(**Figure 5 C**) and the corresponding maximum fluorescence intensity was λ_{max} = 610 nm (**Figure 5 C**), indicating the presence of Doxo. Furthermore, the relaxation time of the nanomedicine was also tested. The measured T1 of the nanomedicine was very high in comparison to T2. The T1 = 351 ms (**Figure 5 E**) was because the signals from Gd were quenched in presence of IONP. Correspondingly the T2 tested was noted to be T2 = 85 ms (**Figure 5 F**), indicating the presence of strong magnetic nanoparticles. Taken together, the characterization data indicates successful synthesis of the IONP-Doxo-SS-Gd-ICAM1 solution.

2.6.2) Characterization of IONP-Doxo-SS-Gd-PD-L1:

To assess the properties of IONP-Doxo-SS-Gd-PD-L1, various characterization tests were performed. Firstly, the size and surface charge were tested. The diameter of IONP-Doxo-SS-Gd-PD-L1 was determined to be D = 98 ± 2 nm (**Figure 6 A**) and subsequent surface charge was -16 ± 3 mV (**Figure 6 B**). These results represent successful conjugation. In addition to this, the presence of Doxo-SS-Gd was tested using absorbance and fluorescence studies. The maximum absorbance was noted to be λ_{abs} = 490 nm (**Figure 6 C**) and emission maxima was λ_{max} = 595 nm (**Figure 6 D**), signifying the presence of Doxo. To detect the activity of Gd in IONP-Doxo-SS-Gd-PD-L1, the relaxation time was measure. The T1 value was noted to be T1 = 254 ms and the T2 determined was 74 ms.

As expected the T1 MR signal of Gd is reduced due to the presence of strong T2 MR signals of IONP. Hence, all the characterization results reveal the successful assembly of IONP-Doxo-SS-Gd-PD-L1.

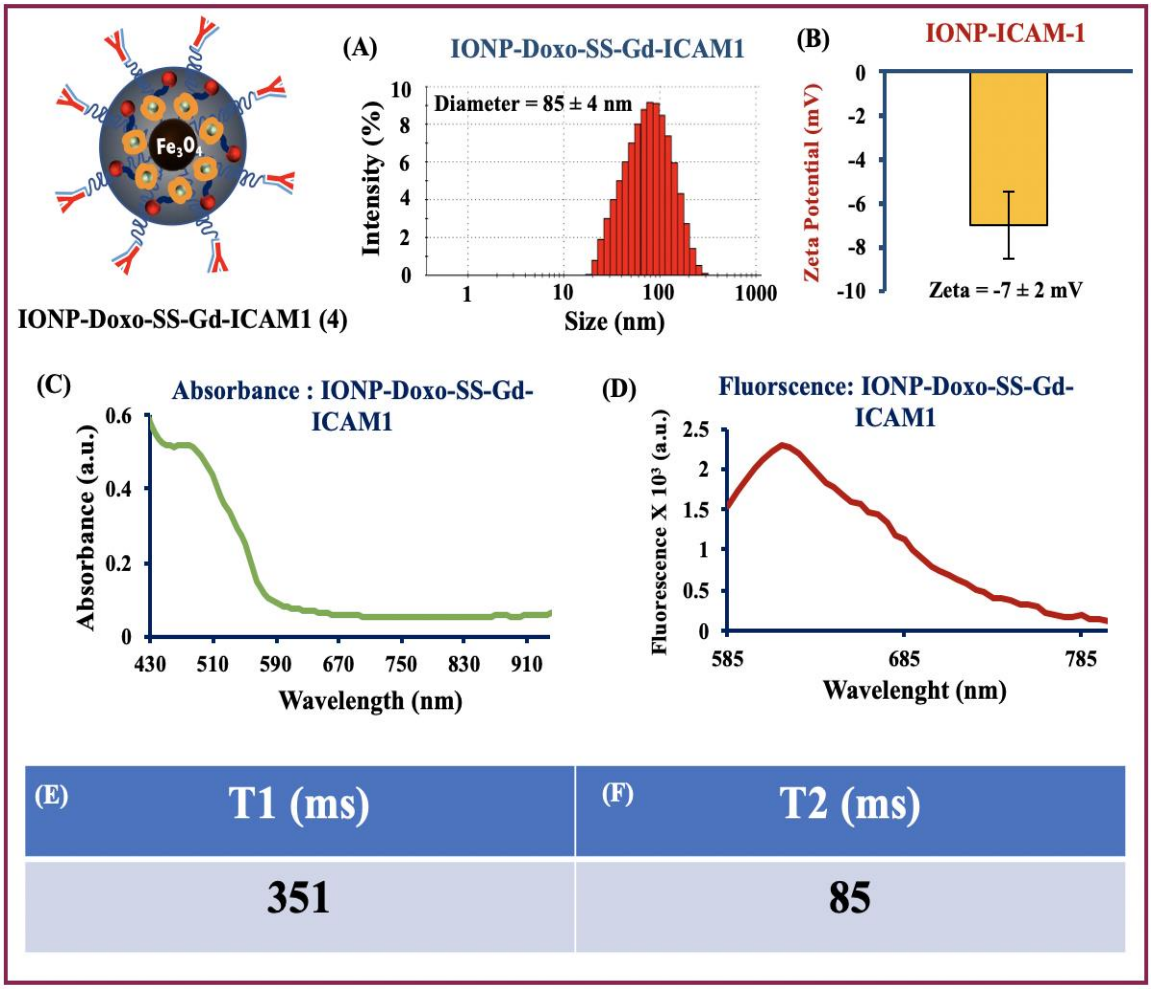

Figure 5: Characterization studies of IONP-Doxo-SS-Gd-ICAM1. (A) Size distribution found to be 85 ± 4 nm. (B) Surface zeta potential measure was -20 ± 1 mV. (C) Absorbance maximum was discovered to be λ_{abs} = 490 nm and (D) the fluorescence maximum was found to be λ_{max} = 610 nm. (E) The T1 measured was 490 nm and (F) T2 signals were determined to be 85 ms. All the characterization results indicated the successful synthesis of IONP-Doxo-SS-Gd-ICAM1.

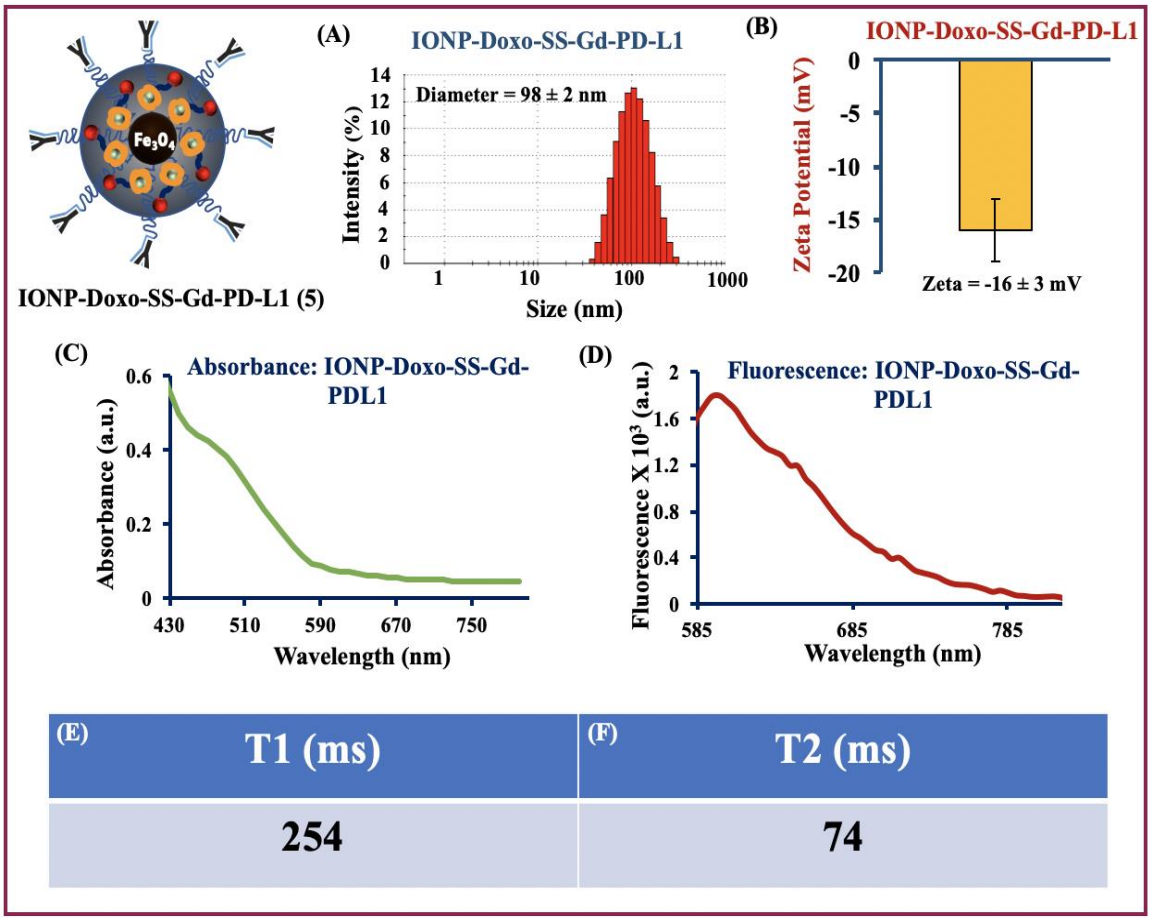

Figure 6: The characteristics of IONP-Doxo-SS-Gd-PD-L1 were studies by various techniques. DLS studies indicated (A) the diameter changed to 98 ± 2 nm and (B) the zeta potential was –16 ± 3 mV. Fluorescence studies denoted the (C) absorbance to be λ_{abs} = 480 nm and (D) fluorescence maxima was λ_{max} = 595 nm. Furthermore, the MR studies suggested the (E) T1 signals T1= 254 ms and the (F) T2 relaxation was T2 = 74 ms. Characterization studies ascertains the synthesis of IONP-Doxo-SS-Gd-PD-L1 was successful.

2.7) Imaging property of IONP-Doxo-SS-Gd-PD-L1:

Gd-DTPA complex is a T1 active agent responsible for bright contrast images in MRI. When Gd-DTPA is encapsulated inside the IONP, the T1 property of gadolinium is quenched due to the strong T2 MR signals from IONP. Upon internalization in the cell Doxo-SS-Gd prodrug is release due to the acidic microenvironment, resulting in strong T1 signals and corresponding bright contrast. Therefore, the activity of Gd in IONP-Doxo-SS-Gd-PD-L1 was examined at pH= 5.0 via MR imaging. To obtain the MRI images of the IONP-Doxo-SS-Gd-PD-L1, six different solutions having varied concentration of Gd and IONP were prepared. The T1 and T2 of the system were measured, before and after incubation in pH = 5.0 (**Figure 7**) using a B = 9.3 T MRI machine at Hoglund brain imaging center at University of Kansas Medical Center. The experiment indicated that with increasing the IONP concentration the T2 MR signals get stronger and the dark contrast increases. The T2 remains active before and after the incubation at pH = 5.0 (**A, Figure 8**). This result indicated the strong T2 MR property of IONP is not quenched upon encapsulation with the prodrug. On the other hand, when the T1 signals of the same sample were measured, before addition of the nanosystem in pH = 5.0 the prodrug resided in the cavities of IONPs and, no change in the T1 contrast was observed (**A, Figure 8**). But once the IONP-Doxo-SS-Gd-PD-L1 (**5, Scheme 2**) is introduced to pH = 5.0, bright contrast images were obtained. As seen in **A, Figure 7** the T1 signals increased resulting in enhanced bright contrast, as the concentration of Gd increased in the nanoparticles. Therefore, this experiment demonstrates the unique activatable (OFF/ON) T1 MR property of our nanosystem in can be used for the diagnosis and treatment monitoring of cancer.

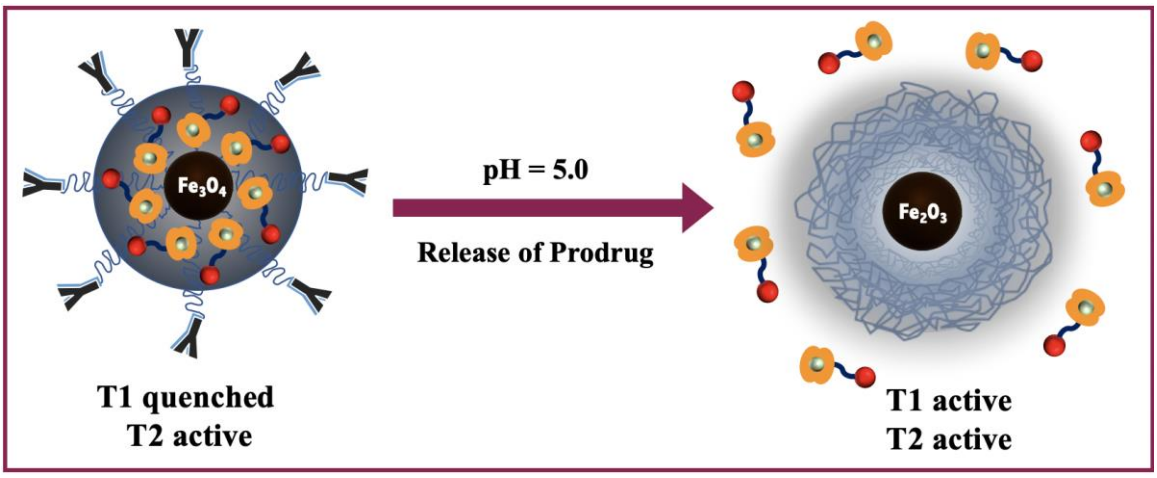

Figure 7: Schematic representation of the changes in T1/T2 signals before and after incubation of the nanomedicine in pH = 5.0

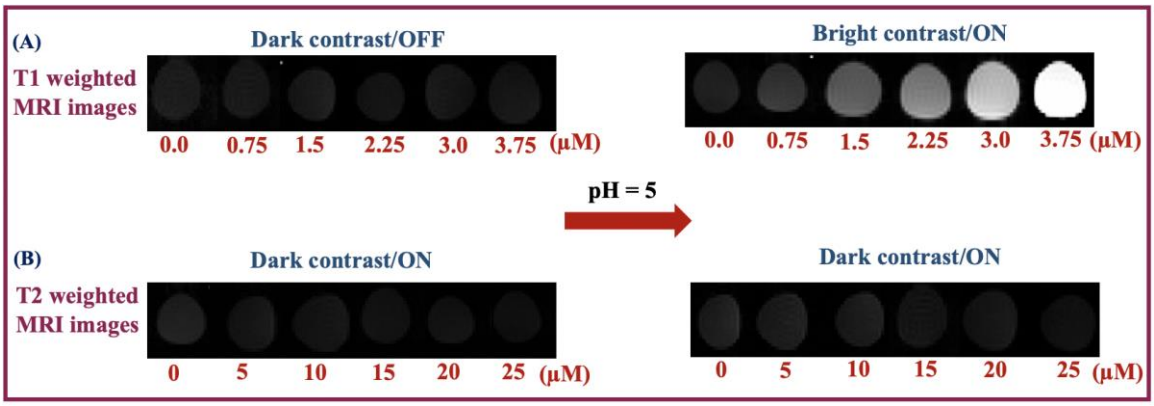

Figure 8: Imaging of IONP-Doxo-SS-Gd-PD-L1 using MRI technique. (A) With increase in the concentration of Gd, the T1 signals get stronger and the bright contrast increase at pH = 5.0. (B) T2 weighted images represent the enhanced dark contrast before and after incubation with pH = 5.0.

2.8) Stimulation of PD-1 on jurkat cells:

Most of the T-cells are known to have PD-1 expression. In this work, we used Jurkat which has limited PD-1 expression. For the overexpression of PD-1 on jurkat cells polyheamagglutinin (PHA) a lectin was used (45). The stimulation was carried out over a time course of 24 and 48 h. Jurkat cells were then labelled with fluorescent active anti-PD-1 antibody. Here the absorbance intensity is a direct measure of the PD-1 overexpression. As seen in **Figure 9**, at 24 h the absorbance of PHA (+) jurkat cells is twice in comparison to the PHA (-) jurkat cells. Correspondingly, at 48 h the absorbance of PHA stimulated jurkat cells was higher in comparison to PHA non-stimulated cells. Hence, this result depicted the successful overexpression of PD-1 on jurkat cells upon stimulation.

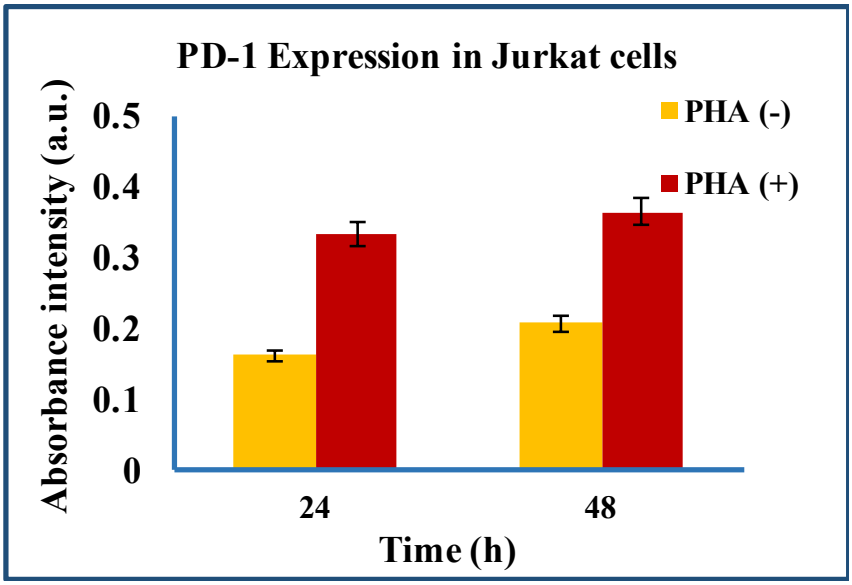

Figure 9: The absorbance intensity of PHA (-) and PHA (+) jurkat cells at 24 and 48 h. At 24 h, the PHA (-) have less absorbance in comparison to PHA (+). Similar results were obtained for jurkat cells at 48 h.

2.9) Cytotoxic assay of MDA-MB-231 & MCF-7:

MTT assay is a standard technique to quantify the cytotoxicity of different therapeutic compounds. The principle of MTT is based on, the yellow colored MTT solution transforms to purple color formazons crystals, in of enzyme mitochondrial reductase present found in the viable cells. However, in dead cells the concentration of this enzyme is so low that reduction of MTT to its insoluble formazon does not take place. Absorbance intensity of the formazons is therefore directly proportional to the live cells. Three different nanoformulations were tested for the immunotherapeutic and chemotherapeutic potential. The solutions tested were 1) IONP-PD-L1 (**2, Scheme 2**) which was responsible for generating immune response while, 2) IONP-Doxo-SS-Gd-ICAM1 (**4, Scheme 2**) was accountable for the chemotherapeutic effect and 3) IONP-Doxo-SS-Gd-PD-L1 which help in (**5, Scheme 2**) generating a chemo-immunotherapeutic response. Cell viability of MDA-MB-231 was measure for 24 h and 48 h post-treatment with these three different nanoformulations ([Fe] = 1mM). As seen in **Figure 10 A**, at 24 h, IONP-PD-L1 (**2, Scheme 2**) and IONP-Doxo-SS-Gd-ICAM1(**4, Scheme 2**) both showed 70% - 75% viability, which was higher in comparison to the viability of IONP-Doxo-SS-Gd-PD-L1 (60 % viable cells). In contrast to this, the viability of the control cells was almost 100% at both 24 h and 48 h, signifying immune cells even if are present, won't attack the cancer cells as the PD-1 & PD-L1 interaction is taking place. Furthermore, at 48 h the viability of IONP-Doxo-SS-Gd-ICAM1 (**4, Scheme 2**) and IONP-PDL1 (**2, Scheme 2**) were found to be 36% and 50%, respectively. Doxo is known to break DNA strands via acting on Topoisomerase II at around 48 h. Due to this reason, there is a drastic decrease in the cell viability from 24 h to 48 h upon treatment with IONP-Doxo-SS-Gd-ICAM1.

The treatment with IONP-Doxo-SS-Gd-PD-L1(**5, Scheme 2**) however, showed 20 % viable cells. This result shows the potential of IONP-Doxo-SS-Gd-PD-L1, which has the combined immunotherapeutic as well as and chemotherapeutic effect.

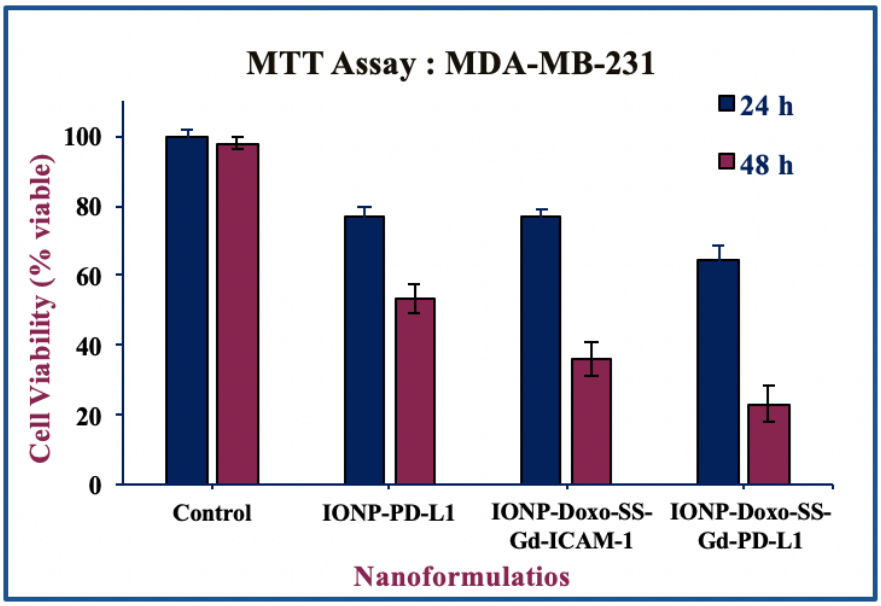

Figure 10 A. Cell viability assay of MDA-MB-231 when treated with three different nanoformulations for 24 h and 48 h. Maximum cell death was found at 48 h in combination treatment.

Similarly, the MTT assay was performed for control cell MCF-7. It is a type of breast cancer cell line lacking PD-L1 receptor and has a little ICAM-1 expression. IONP-PD-L1 (**2, Scheme 2;** [Fe] = 1 mM), IONP-Doxo-SS-Gd-ICAM1 (**4, Scheme 2;** [Fe] = 1 mM) and IONP-Doxo-SS-Gd-PD-L1 (**5, Scheme 2;** [Fe] = 1 mM) were tested ffor 24 and 48 h. As seen in **Figure 10 B** the cell viability remains fairly high after 24 h and 48 h due to absence of PD-L1 receptor on the surface of MCF-7. Although, after treating the cells with IONP-Doxo-SS-Gd-ICAM-1 there was a slight reduction in viability due to some

overexpression of ICAM-1 receptor on the surface of MCF-7. Overall this study signifies the specificity of our nanosystem in targeting the desired cancer cells.

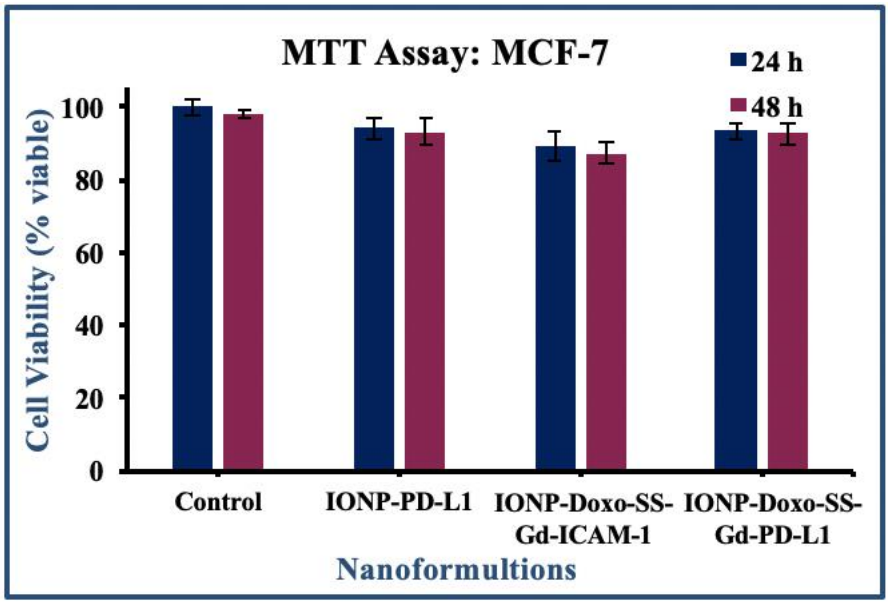

Figure 10 B: Cell viability assay for MCF-7 upon treatment with different nanoformulations for 24 h and 48 h. The viability remains fairly constant due to absence of PD-L1 receptor on the surface.

2.10) Fluorescence studies:

To visually assess the cell death of MDA-MB-231, fluorescence studies were carried out. Three different nanoformulations of, IONP-PD-L1 (**2, Scheme 2;** [Fe] = 1 mM), IONP-Doxo-SS-Gd-ICAM1 (**4, Scheme 2;** [Fe] = 1 mM) and IONP-Doxo-SS-Gd-PD-L1 (**5, Scheme 2;** [Fe] = 1 mM) were tested for 24 h and 48 h to visually evaluate the changes in cell morphology. Doxorubicin in a known fluorophore and therefore, it can fluoresce once it enters the cancer cells. Furthermore, we stained the nucleus with DAP1 to better understand the cells morphology. The IONP-PD-L1 formulation does not have Doxorubicin and so, we encapsulated DiI in order to observe the fluorescence in this

nanoformulation. At 24 h, it was observed upon treatment with IONP-PD-L1 (**2, Scheme 2**) fewer cells underwent morphological changes indicating the effect of IONP-PD-L1 on the viability of cells (**Figure 11 A-D**). Furthermore, when cells were treated with IONP-Doxo-SS-Gd-ICAM1 (**4, Scheme 2**; **Figure 11 E-H**), fewer cells showed the signs of being unhealthy, because Doxo acts at near to 48 h. Subsequently, when cells were treated with IONP-Doxo-SS-Gd-PD-L1 (**5, Scheme 2**; **Figure 11 E-H**) a synergistic effect of chemoimmunotherapy was observed and, many cells exhibited the signs of being unhealthy. This result proved IONP-Doxo-SS-Gd-PD-L1 treatment was very effective and also reinforces our MTT assay at 24 h.

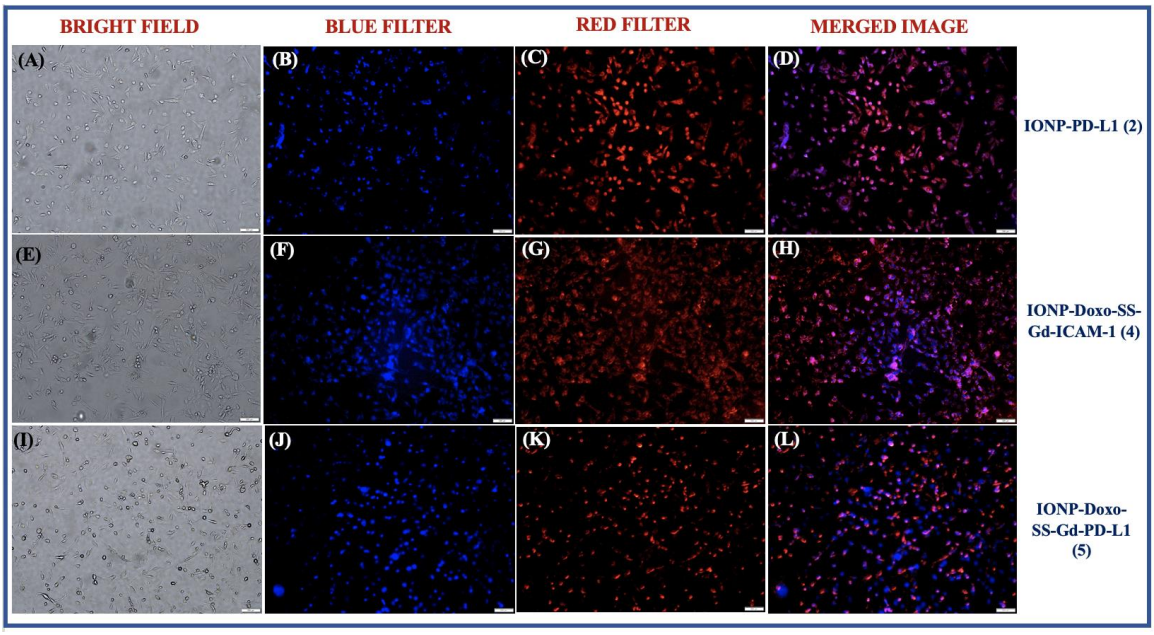

Figure 11. Cell based fluorescence studies for 24 h: A-D is a representation of cells after treatment with IONP-PD-L1, E-H represents treatment of MDA-MD-231 with IONP-Doxo-SS-ICAM-1 & I-L are the microscopic images of MDA-MB-231 upon treatment with IONP-Doxo-SS-Gd-PD-L1 using blue filter (for DAPI) and red filter (for Doxo).

Similarly, fluorescence based studies were carried out at 48 h using the nanoformulations mentioned above. It was observed that at 48 h, most of the cells were dying in presence of IONP-PD-L1 (**Figure 12 A-D**), indicating the effect of immunotherapy on cancer cells. Moreover, when cells were treated with IONP-Doxo-SS-Gd-ICAM-1 (**Figure 12 E-H**), due to Doxo's action, the cell density was reduced and most of them experienced cell death. In comparison to this, when MDA-MB-231 was subjected to IONP-Doxo-SS-Gd-PD-L1 (**Figure 12 I-L**), a drastic decrease in the cell density and cell viability was observed indicating the potent effect of chemoimmunotherapy. All these results reinforce that our nanosystem is very efficient in killing cancer cells and using the combined chemoimmunotherapy approach.

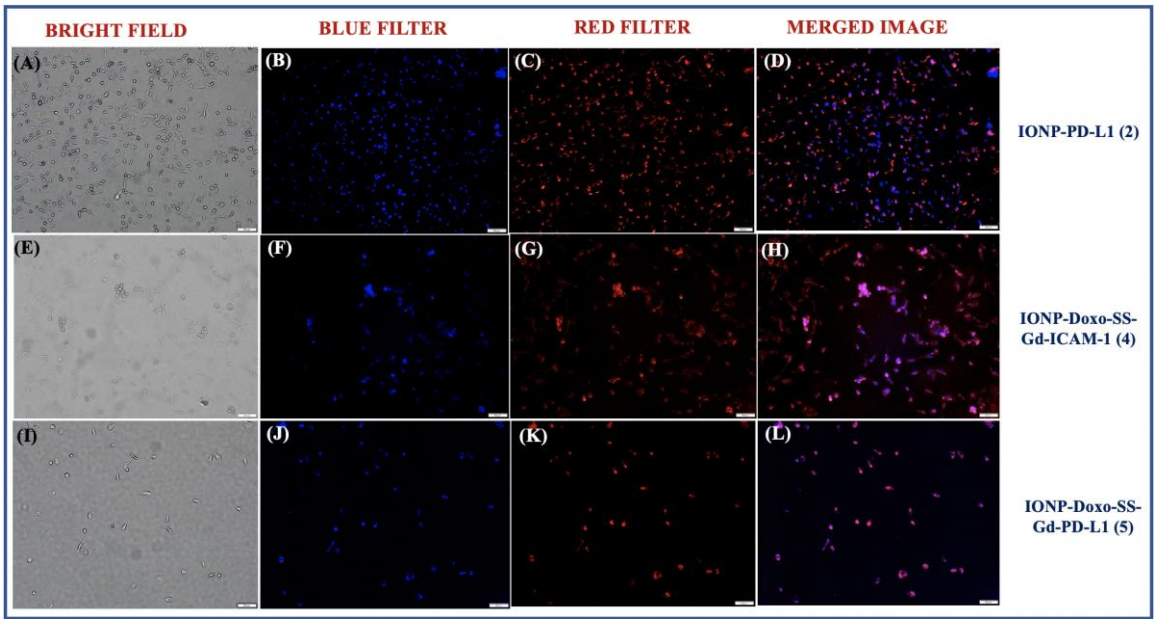

Figure 12. Cellular studies for MDA-MB-231 at 48 h: Images A-D denotes the treatment with IONP-PD-L1, figures E-H are a representation of cells treated with IONP-Doxo-SS-Gd-ICAM-1 and images I-L are the images of cells upon treatment with IONP-Doxo-SS-Gd-PD-L1.

2.11) Cellular apoptosis measurement:

Apoptosis is a programed cell death. MDA-MB-231 cells undergo apoptosis due to the attack from the immune system and the therapeutic drug. In apoptotic cells, phosphotidylserine a phospholipid existing in the inner leaflet of the cells, moves to the outer leaflet of the cells. Phosphatidylserine has a high affinity for a protein Annexin-V. In this assay, the protein is labeled with FITC dye to fluoresce the apoptotic cells once the labeled protein attaches to the apoptotic cells. The cellular apoptosis of MDA-MB-231 was tested at 24 h post treatment with different nanoformulations. As seen in **Figure 13 A-B** the treatment with IONP-PD-L1 shows certain cells are fluorescing indicating apoptosis. Furthermore, MDA-MB-231 when treated with IONP-Doxo-SS-Gd-ICAM1 has less apoptotic cells (**Figure 13 C-D**) because Doxo acts at around 48 h of treatment. Lastly, the maximum apoptosis was noted when cells were incubated with IONP-Doxo-SS-Gd-PD-L1 (**Figure 13 E-F**) due to the dual action of drug and immune cells. This result further validates our previous cytotoxicity assay and additionally proves the potential of nanosystem in eradicating cancer cells. A similar set of experiment was carried out at 48 h. It was observed that, when MDA-MB-231 was treated with IONP-Doxo-SS-Gd-PD-L1 for 48 h, the cell density decreased (**Figure 14 C**) and most of the cells were apoptotic. Furthermore, in IONP-Doxo-SS-Gd-ICAM1 treatment the cell density (**Figure 14 C**) was lower than that of IONP-PD-L1 treatment but, the level of apoptosis increase (**Figure 14 A-B**) in comparison to 24 h treatment. In the IONP-Doxo-SS-Gd-PD-L1 treatment, as seen in **Figure 14 E**, the cell density was minimal and the level of apoptosis (**Figure 14 F**) was relatively high when compared to the 24 h treatment. This results shows the capability of our nano-platform to effectively kill cancer cells

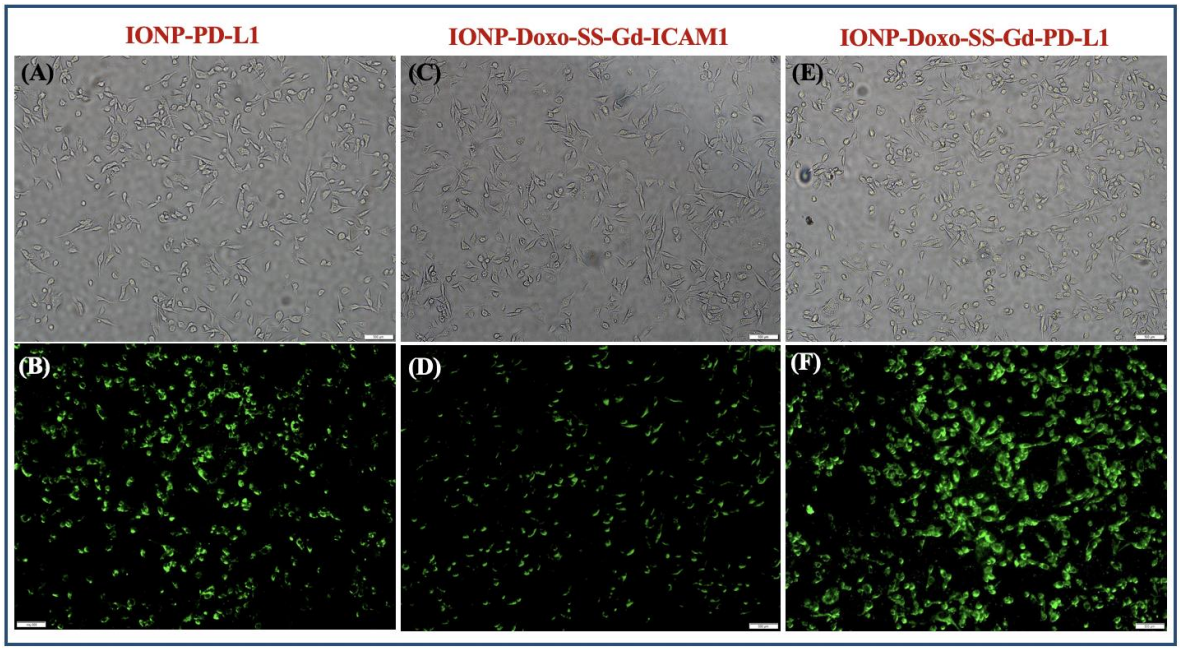

Figure 13. Cellular apoptosis at 24 h in presence of different nanoformulations. A, C and E are the bright field representations of apoptotic cells and B, D and F are Annexin-FITC labeled cells which are fluorescing green.

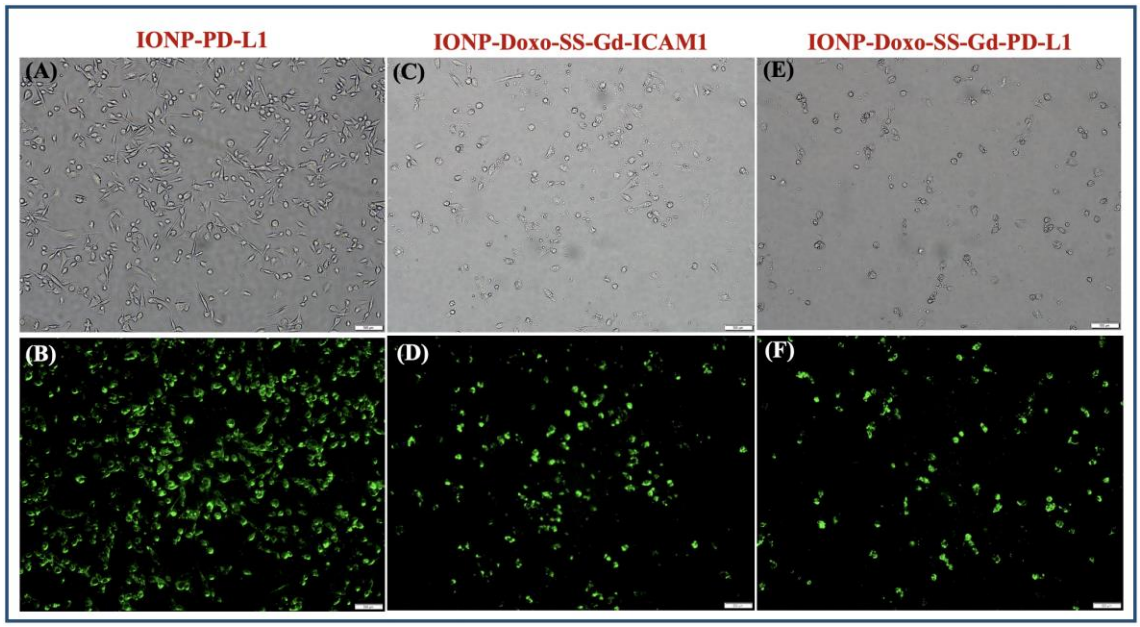

Figure 14: Here, A-B represents the cellular apoptosis when treated with IONP-PD-L1, C-D are a representation of apoptotic cells post treatment with IONP-Doxo-SS-Gd-ICAM1 and, E-F represent the apoptosis experience by cells after treatment with IONP-Doxo-SS-Gd-PD-L1.

2.12) Determining Human IL-2 level:

The PD-1 and PD-L1 interaction is responsible for generating negative immune response via inhibiting the antitumor activity of T cells. Immune checkpoint inhibition of PD-1 and PD-L1 interaction plays a major role in cancer immunotherapy. PD-1/PD-L1 antibodies have proved to increase cancer patient's survival and improve their life quality. Therefore, to achieve an immunotherapeutic response from the Jurkat cells, anti PD-L1 Ab was used for obstructing this interaction. The interaction of PD-1 with PD-L1, leads to suppression of lymphocytes proliferation and cytokines secretion but, by impeding the PD-1 and PD-L1 engagement via anti-PD-L1 Ab can lead to elevated Interleukin-2 (IL-2) production. The IL-2 secretion help stimulate the immune cells to attack cancer cells. (45)

2.12.1) IL-2 standard calibration curve.

For measuring the unknown IL-2 concentration, firstly a standard calibration curve was obtained, from which undetermined IL-2 concentration could be quantified. To perform this calibration, IL-2 standards of known concentrations were obtained and, seven different serial dilutions were made from the standard stock. Using this serially diluted solutions ELISA was carried out following the instructions provided by the manufacturer, followed by measuring absorbance from at 450 nm. The absorbance of the samples was directly proportional to the concentration of the IL-2. As seen in **Figure 15**, the absorbance verses IL-2 level implied to have a liner relationship indicating the successful calibration. This calibration curve would help us in determining the IL-2 concentration in samples treated with various nanoformulations.

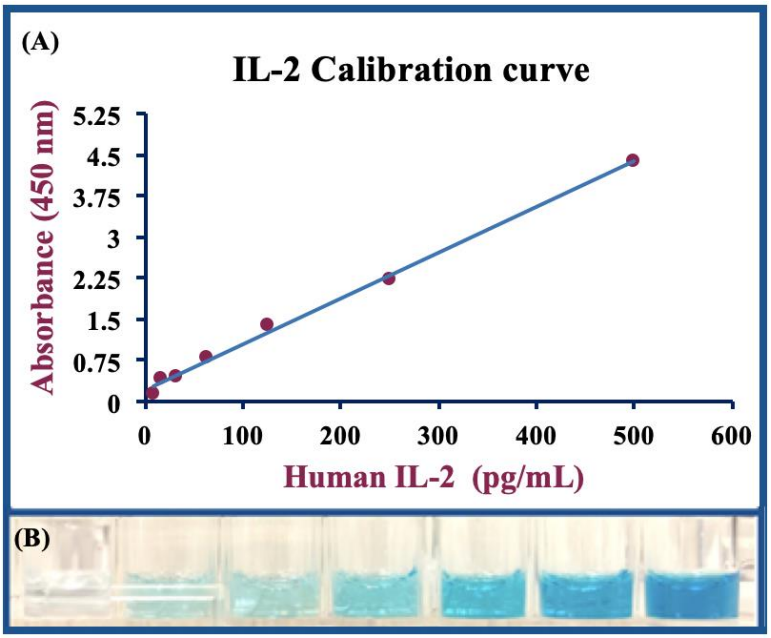

Figure 15: (A) IL-2 calibration curve indicates with increase in the IL-2 concentration the absorbance intensity increases and a liner relationship is obtained. (B) Furthermore, the increase in the color intensity also implies the increase in concentration of IL-2

2.12.2) IL-2 level after treatment with different nanoformulations.

As discussed earlier, IL-2 levels increase upon obstructing the interaction of PD-1 & PD-L1. To test the changes in IL-2 level upon subjecting the cells with different nanoformulations, ELISA was carried out. Firstly, the co-cultured cells were exposed to three different nanoformulations of, IONP-PD-L1 (**2, Scheme 2;** [Fe] = 1 mM), IONP-Doxo-SS-Gd-ICAM-1 (**4, Scheme 2;** [Fe] = 1 mM) and IONP-Doxo-SS-Gd-PD-L1 (**5, Scheme 2;** [Fe] = 1 mM) for 24 h. Besides this a control condition was maintained, where the co-culture was devoid of any treatment. In the controlled condition the IL-2 levels (7.2 pg/mL) were minimum, indication the suppression of IL-2 secretion upon PD-L1 an PD-1 interaction. On the other hand, upon treatment with IONP-PD-L1 the IL-2 levels were

noted to be elevated (23.39 pg/mL), due to the blocking of PD-1: PD-L1 interaction (**Figure 16**). The results obtained for IL-2 level upon testing IONP-Doxo-SS-Gd-PD-L1 were very speculative. We anticipated low IL-2 levels as there is no anti-PD-L1 ligand attached although, we later on discovered that Doxo itself induced IL-2 production in the co-culture system but, the mechanism of this event it unknown. Therefore, the slight increases in the IL-2 level (18.99 pg/mL) upon IONP-Doxo-SS-Gd-ICAM1(**Figure 16**) treatment is due to Doxo. Additionally, the IL-2 levels (31.09 pg/mL) upon treatment with IONP-Doxo-SS-Gd-PD-L1 were higher compared to the other two systems (**Figure 16**), indicating the combined IL-2 production from Doxo and anti-PD-L1. This result further validates the potential of nanosystem in treating the cancer cells using a combined chemoimmunotherapy approach.

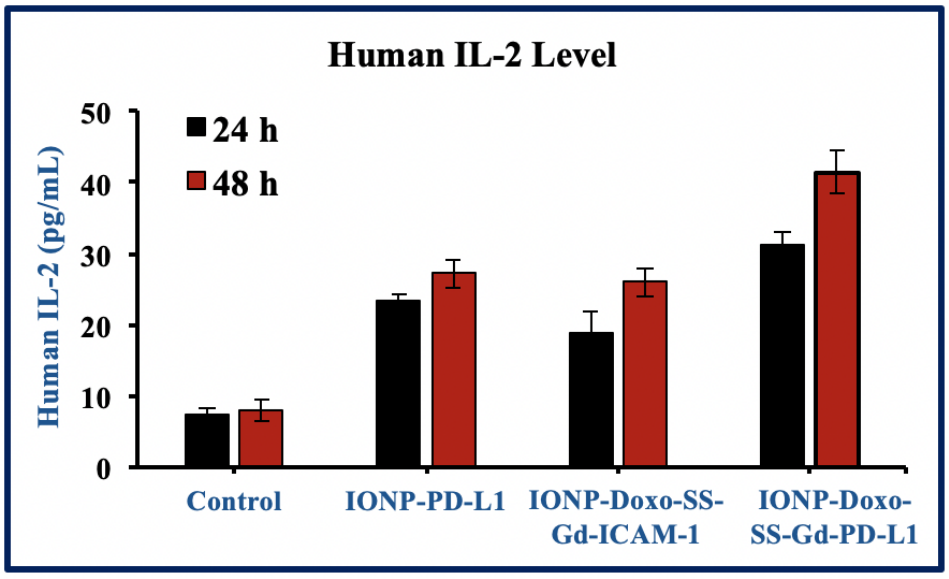

Figure 16: IL-2 level upon treatment with IONP-PD-L1, IONP-Doxo-SS-Gd-PD-L and IONP-Doxo-SS-Gd-ICAM1 at 24 h and 48 h.

Similar sets of experiments were carried out at 48 h for testing the IL-2 levels. It was observed that upon treating the co-cultured medium with IONP-PD-L1 for 48 h, the IL-2 level augmented to 27.17 pg/mL in compared to 24 h treatment. Also upon treating the co-culture system with IONP-Doxo-SS-Gd-ICAM1 a big variation in IL-2 level (26.08 pg/mL) was noted due to presence of Doxo (**Figure 16**). In comparison to this, IONP-Doxo-SS-Gd- PD-L1 had the maximum IL-2 level at 48 h due to the combined effect of anti-PD-L1 and Doxo, intensifying the secretion. These results validate our previous experimental outcomes indicating the potential of chemoimmunotherapy approach in treatment of MDA-MB-231.

Chapter III

Experimental section

1.0) Materials:

Ferric chloride hexahydrate ($FeCl_3.6H_2O$), Ferrous chloride tetrahydrate ($FeCl_2.4H_2O$), N, N-dimethyl sulfoxide (DMSO), Phosphate buffer saline (PBS), ammonium hydroxide (NH_4OH), 10X, Sulfuric acid (H_2SO_4) and Hydrochloric acid (HCl) were obtained from Fisher scientific and stored at appropriate temperature. 2-morpholinoethanesul-fonic acid (MES) and Polyacrylic acid (PAA) were received from Sigma-Aldrich and used without any further purification. 4,6-diamidino-2-phenylindole (DAPI) dye along with Near infrared DiI dye were bought from Invitrogen. ICAM-1 was received from Sino Biological Inc. and stored according to the instructions. Apoptosis and necrosis quantification kit (FITC-Annexin V, Ethidium homodimer III and 5X Annexin V binding buffer) was bought from Biotium and stored for future use. Para-formaldehyde was acquired from electron microscopy science. Jurkat cells, MCF-7 and MDA-MB-231 were obtained from ATCC and thawed upon arrival. DMEM, RPMI, penicillin-streptomycin solution (100X) and Fetal bovine serum (FBS) were also acquired from ATCC. Doxorubicin was purchased from Alexis biochemicals and stored at 4 °C for further use. 1-ethyl-3-(3-(dimethylaminopropyl)carbodiimidehydrochloride (EDC) was obtained from Thermo Scientific while, N-Hydroxy succinimide (NHS) was purchased from ACROS

organics and stored at suitable temperature. Moreover, DSP crosslinker (Dithiobis[succinimidyl propionate]) was obtained from ProteoChem and kept at appropriate temperature. Further 3-(4,5-dimethylth- iazol-2-yl)-2,5-diphenyltetrazolium bromide (MTT) was procured from MP bio medicals and placed in refrigerator. Pacific Blue anti-human CD279 (PD-1) Antibody, Human IL-2 ELISA MAX™ Deluxe and Nunc™ MaxiSorp™ ELISA Plates, Uncoated were purchased from Biolegend and stored at appropriate temperature. Polyheamagglutinin-P NFAT Activator was obtained from Invivogen for stimulation of PD-1.

1.1) Synthesis of Doxo-SS-Gd prodrug

To synthesize Doxo-SS-Gd, three different solutions were prepared. Firstly, 1 mg of Doxo-NH_2 (0.00184 mM) was suspended in 100 μL water followed by dissolving 1.73 mg of Gd-DTPA in 100 μL of water (Doxo-NH_2:Gd-DTPA are in 1:1 ratio). Lastly, 0.744 mg of dithiobis(succinimidyl propionate) (DSP) crosslinker was dissolved in 35 μL of DMSO. All the solutions prepared, were mixed and allowed to react for 1 h at room temperature in presence of Et_3N (10 μL). The product obtained was purified using PD-10 column (Sephadex G-25 resin) to get 25 μM Doxo-SS-Gd prodrug (**Scheme 1**). This prodrug was characterized using TECAN fluorescence plate reader and Bruker benchtop MRI.

1.2) Synthesis of iron oxide nanoparticle (IONP)

For preparing IONPs the following three solutions were made: 1) 0.860 mg of Polyacrylic acid (PAA) dissolved in 5 mL of H_2O, 2) NH_4OH solution (30% of 1.8 mL NH_4OH in 15 mL of water) and 3) iron salts (0.340 mg of $FeCl_2.4H_2O$ and 0.610 mg of

$FeCl_3.6H_2O$) dissolved in 2 mL DI water and 80 μL of 12 N HCl. For starting the synthesis, iron salts solution was added to the solution of NH_4OH at 900 rpm followed by addition of PAA solution. This mixture was vortex for 60 min at 2500 rpm. The solution obtained was further centrifuged at 3000 rpm and 4000 rpm for 20 min. Finally, IONP-COOH supernatant was obtained and purified magnetic column and dialysis technique (dialysis bag MWCO = 6-8 kDa). The purified solution of IONP-COOH (**1, Scheme 2;** [Fe] = 4 mM) characterized using DLS and stored at 4 °C for future use.

1.3) Encapsulation of Doxo-SS-Gd prodrug in IONP using solvent diffusion method.

For synthesizing IONP-Doxo-SS-Gd-COOH (**3, Scheme 1**), a 10 μL of 25 μM Doxo-SS-Gd prodrug was dissolved in 250 μL DMSO. This dilute solution was added to 5 mL of IONP in drop wise manner, ensuring constant vortexing at 1500 rpm. The final product was rested on table mixture for 2 h followed by purification using magnetic column and dialysis against water for 2 h. Subsequently IONP-Doxo-SS-Gd-COOH (**3, Scheme 1**; [Fe] = 2 mM) solution was characterized via fluorescence plate reader and DLS and later on stored at 4 °C.

1.4) Conjugation of ICAM-1 using EDC/NHS chemistry:

To synthesize IONP-Doxo-SS-Gd-ICAM1 (**4, Scheme 2**), EDC/NHS carbodiamide was performed. 12 mg of EDC was dissolved in 250 μL of MES buffer (10 mM). Additional, 8 mg of NHS was added to 250 μL of 10 mM MES buffer, followed by preparing a 5 μL of 0.52 mM ICAM-1 in 250 μL PBS (pH = 7.4). EDC solution was added

in 5 parts to 5 mL IONP-Doxo-SS-Gd-COOH (**3, Scheme 2**; [Fe] = 2 mM) solution followed by addition of NHS in same fashion. This mixture was allowed to react for 3 minutes and finally ICAM-1 solution was added drop wise to obtain IONP-Doxo-SS-Gd-ICAM1 (**4, Scheme 2**). This solution was then purified using magnetic column and dialysis technique. 1 mM IONP-Doxo-SS-Gd-ICAM1 (**4, Scheme 2**) was obtained after purification and it was characterized using Malvern Zeta sizer, TECAN plate reader and Bruker's benchtop MRI for size & zeta potential, absorbance & emission spectra, T1 & T2 relaxation time respectively.

1.5) Synthesis of IONP-PD-L1 & IONP-Doxo-SS-Gd-PD-L1:

For synthesizing IONP-PD-L1 (**2, Scheme 2**) and IONP-Doxo-SS-PD-L1 (**5, Scheme 2**), EDC/NHS chemistry was performed. Firstly, 9 mg of NHS was mixed with 100 μL MES buffer (10 mM) followed by mixing 6 mg of NHS in 100 μL MES buffer. Further 10 μL of 5 μg/mL anti PD-L1 was added to 100 μL of DMSO. To carry out the conjugation, 5 mL of IONP-COOH (**1, Scheme 2**; [Fe] = 2 mM)/IONP-Doxo-SS-Gd-COOH (**3, Scheme 2**; [Fe] = 2 mM) was pipetted out and, EDC was added to the solution in 5 parts. Subsequently, NHS was added in a similar fashion and the mixture was allowed to react for 3 minutes. Later on, anti-PD-L1 solution was added to the reaction mixture in 10 parts. Finally, a solution of IONP-PD-L1 (**2, Scheme 2**) and IONP-Doxo-SS-Gd-PD-L1 (**5, Scheme 2**) was obtained and purified using magnetic column and dialysis technique. After purification the solutions of IONP-PD-L1 (**2, Scheme 2**; [Fe] = 1 mM) and IONP-Doxo-SS-Gd-PD-L1 (**5, Scheme 2**; [Fe] = 1 mM) were characterized using DLS, fluorescence plate reader and benchtop MRI.

1.6) MR imaging studies:

To carry out MR imaging studies a stock solution of IONP-Doxo-SS-Gd-PD-L1 was prepared ([Doxo-SS-Gd] = 25 μM & [IONP] = 2 mM). Form this solution five different dilutions were prepared where the concentration of Gd was 0.75, 1.5, 2.25, 3.0 and 3.75 μM for T1 based MR imaging. Similarly, IONP dilutions were prepared with concentrations to be 5, 10, 15, 20 and 25 mM for T2 based MR imaging. This study was performed in MRI machine (B = 9.3 T) at Hoglund brain imaging center, KUMC.

1.7) MALDI Matrix Preparation:

1. Preparation of TA30 Solvent:

   TA30 is a 30:70 (vol/vol) mixture of acetonitrile (ACN): trifluoroacetic acid (TFA) in deionized water. The solutions were combined in volumes where, 300 μL ACN + 699.3 μL deionized water + 0.7 μL TFA = 1 mL TA30 solvent.

2. Matrix Solubilization:

   2, 5-Dihydroxybenzoic acid (20 mg/mL) was added to the TA3O solution and allowed to dissolved.

3. Sample Preparation:

   50 mg/mL methanol was used to dissolve the prodrug

4. Sample Plating:

   Equal volumes of matrix solution and prodrug solution were mixed into a new tube and vortexed for a few minutes until thoroughly mixed. Then, 0.5 μL drop of

this solution was placed on the MALDI plate. The sample was allowed to completely air dry in the hood overnight.

1.8) Overexpression of PD-1:

Polyheamagglutinin (PHA) was used for the overexpression of PD-1 on jurkat cells. The cells were seeded in a 96 well plate along with 10 μL of 10 μg/mL PHA for 24 h and 48 h. After the incubation period was over the cells were labelled with 10 μL Pacific blue anti PD-1 (10 μg/100 μL) for 15 minutes. Later on, the cells were washed with 1 X PBS and centrifuged at 1200 rpm. The cell pellet obtained was re-suspended in PBS and absorbance was measured 405 nm.

1.9) Co-culture of MDA-MB-231 and Jurkat cells.

MDA-MB-231 was trypsinized and seeded in a 12 well plate and placed in the incubator (37 °C, 5 % CO_2) for 24 h. On the same day, jurkat cells were centrifuged and seeded in 12 well plate with PHA for overexpression and incubated for 24 h. Jurkat cells are floating in the media suspension, so they can just be centrifuged to obtain cell pellet. After 24 h incubation time, jurkat cells were centrifuged and added to MDA-MB-231 wells, in 1:5 ratio (MDA-MB-231: Jurkat cells) for co-culture. Furthermore, after 24 h incubation of both the cell in co-culture, different experiments were performed.

1.10) MTT Assay:

For performing MTT assay, MDA-MB-231 and jurkat cells were co-cultured in 4 different wells of a 12 well plate. Subsequently, 200 μL all three nanoformulations of

IONP-PD-L1 (**2, Scheme 2**; [Fe] = 1 mM), IONP-Doxo-SS-Gd-ICAM-1 (**4, Scheme 2**; [Fe] = 1 mM) and IONP-Doxo-SS-Gd-PD-L1 (**5, Scheme 1**; [Fe] = 1 mM) were incubated for 24 h and 48 h. After the treatment period, the media suspension having jurkat cells was removed from the plate and, cells were washed with 1X PBS. Subsequently, 200 μL of 5 mM MTT solution was added and plates were placed in the incubator (37 °C, 5 % CO_2) for 4-6 h. Purple colored formazan crystals were produced and solubilized with the help of acidic isopropyl alcohol. Readings were measured at 520 - 570 nm using the TECAN microplate reader. Similar procedure was carried out and MTT assay was performed for control cells MCF-7.

1.11) Cell based fluorescence studies:

Fluorescence studies were carried out for MD-MB-231 treated with IONP-PD-L1 (**2, Scheme 2**; [Fe] = 1 mM), IONP-Doxo-SS-Gd-ICAM-1 (**4, Scheme 2**; [Fe] = 1 mM) and IONP-Doxo-SS-Gd-PD-L1 (**5, Scheme 2**; [Fe] = 1 mM). Firstly, cells were co-culture in three different wells and then successively treated with 200 μL of different nanoformulations nano-formulations for 24 h and 48 h. Post treatment period, the cells were fixed using 4 % paraformaldehyde for 15 minutes. Subsequently, the nucleus of the cells was stained using DAPI dye (6-diamidino-2-phenylindole, 5 mg/mL) for 10 minutes. The images were obtained using Olympus 1 X 73 fluorescence microscope.

1.12) Cellular apoptosis:

Apoptosis assay quantification kit was used to determine apoptotic cells. MDA-MB-231 and jurkat cells were co-cultured in a 12 well plate for 24 h (37 °C, 5 % CO_2). All

the plates were different nanoformulations. 200 μL of IONP-PD-L1 (**2, Scheme 2**; [Fe] = 1 mM), IONP-Doxo-SS-Gd-ICAM-1 (**4, Scheme 2**; [Fe] = 1 Mm) and IONP-Doxo-SS-Gd-PD-L1 (**5, Scheme 2**; [Fe] = 1 Mm) were added to 3 different wells for 24 and 48 h. Post treatment period, the cells were washed with 2 mL of 1 X binding buffer and stained with 7 μL of FITC dye for 15 min. Then cells were rinsed with 1 X binding buffer and fixed with 5 % paraformaldehyde for 10 minutes. Post fixation cells were washed with 1 X binding buffer and fluorescence images were acquired in fluorescence microscope.

1.13) Detection of IL-2 using ELISA

To test the level of IL-2, ELISA was carried out. First off, a standard calibration curve was obtained from known concentration of serially diluted IL-2 standard. The stock solution had a concentration of 500 pg/mL. From this stock solution, serially diluted samples with concentration of 250 pg/mL, 125 pg/mL, 62.5 pg/mL, 31.3 pg/mL, 15.6 pg/mL and 7.8 pg/mL were prepared. Subsequently, all solutions required for performing ELISA were prepared and stored following the manufactures instructions. Furthermore, the wells were pre-coated with primary antibody and store for 16 -18 h at 4 °C. After performing all the former steps, the latter parts were carried out following the user manual from the manufacturer. The values obtained were then plotted in excel. Similarly, to test the IL-2 level from unknown samples, four different sets of conditions were carried out in co-culture for 24 h and 48 h. The different sets are: 1) No treatment, 2) IONP-PD-L1 (**2, Scheme 2**; [Fe] = 1 Mm), 3) IONP-Doxo-SS-Gd-ICAM1 (**4, Scheme 2**; [Fe] = 1 Mm) and 4) IONP-Doxo-SS-Gd-PD-L1 (**5, Scheme 2**; [Fe] = 1 Mm). Post the treatment period, the cell suspension was obtained and centrifuged at 1200 rpm for 5 minutes. Subsequently, the

cell supernatant was obtained and used to test the IL-2 levels. After obtaining the supernatant the experiment was carried out using the manufacturers user manual.

Chapter IV

Conclusion and Future Directions

In this work, we successfully tested the potential of IONP-Doxo-SS-Gd-PD-L1 by performing various cell-based tests. All the experiments indicated the potential of nanoformulation in generating a combined chemoimmunotherapeutic response for killing the MDA-MB-231 cells. Additionally, the tests done using MR imaging, proved the nanoformulation has the potential to diagnose cancer and further can also monitor the treatment. Hence, our nanoparticles proved to be an excellent model for targeted dual treatment (chemotherapy and immunotherapy) and diagnosis of TNBC cells.

Moreover, this model can be tailored for targeting specific types of tumor and further test its ability in treatment and imaging of the same. After a firm establishment in in-vitro settings, this model can be tested in-vivo to better understand its functioning once inside a living organism. In conclusion, this model has the potential to be examined for various kinds of tumors for its dual targeted treatment and diagnosis purposes.

References

1) Mignani, S.; Bryszewska, M.; Klajnert-Maculewicz, B.; Zablocka, M.; Majoral, J. Advances In Combination Therapies Based On Nanoparticles For Efficacious Cancer Treatment: An Analytical Report. *Biomacromolecules* 2014, *16*, 1-27.

2) Cuenca, A.; Jiang, H.; Hochwald, S.; Delano, M.; Cance, W.; Grobmyer, S. Emerging Implications Of Nanotechnology On Cancer Diagnostics And Therapeutics. *Cancer* 2006, *107*, 459-466.
3) Li, L.; Pang, X.; Liu, G. Near-Infrared Light-Triggered Polymeric Nanomicelles For Cancer Therapy And Imaging. *ACS Biomaterials Science & Engineering* 2017, *4*, 1928-1941.
4) de Jong, W.; Borm, P. Drug Delivery And Nanoparticles: Applications And Hazards. *International Journal of Nanomedicine* 2008, *3*, 133-149.

5) Ho, B.; Pfeffer, C.; Singh, A. Update On Nanotechnology-Based Drug Delivery Systems In Cancer Treatment. *Anticancer Research* 2017, *37*, 5975-5981.

6) Abedi-Gaballu, F.; Dehghan, G.; Ghaffari, M.; Yekta, R.; Abbaspour-Ravasjani, S.; Baradaran, B.; Ezzati Nazhad Dolatabadi, J.; Hamblin, M. PAMAM Dendrimers As Efficient Drug And Gene Delivery Nanosystems For Cancer Therapy. *Applied Materials Today* 2018, *12*, 177-190.
7) Wang, H.; Huang, Q.; Chang, H.; Xiao, J.; Cheng, Y. Stimuli-Responsive Dendrimers In Drug Delivery. *Biomaterials Science* 2016, *4*, 375-390.
8) Wolinsky, J.; Grinstaff, M. Therapeutic And Diagnostic Applications Of Dendrimers For Cancer Treatment☆. *Advanced Drug Delivery Reviews* 2008, *60*, 1037-1055.
9) Pan, J.; Mendes, L.; Yao, M.; Filipczak, N.; Garai, S.; Thakur, G.; Sarisozen, C.; Torchilin, V. Polyamidoamine Dendrimers-Based Nanomedicine For Combination Therapy With siRNA And Chemotherapeutics To Overcome Multidrug Resistance. *European Journal of Pharmaceutics and Biopharmaceutics* 2019, *136*, 18-28.
10) Voit, B. Hyperbranched Polymers: A Chance And A Challenge. *Comptes Rendus Chimie*2003, *6*, 821-832.
11) Santra, S.; Kaittanis, C.; Perez, J. Aliphatic Hyperbranched Polyester: A New Building Block In The Construction Of Multifunctional Nanoparticles And Nanocomposites. *Langmuir* 2010, *26*, 5364-5373.

12) Al-Jamal, W.; Kostarelos, K. Liposomes: From A Clinically Established Drug Delivery System To A Nanoparticle Platform For Theranostic Nanomedicine. *Accounts of Chemical Research* 2011, *44*, 1094-1104.

13) Sercombe, L.; Veerati, T.; Moheimani, F.; Wu, S.; Sood, A.; Hua, S. Advances And Challenges Of Liposome Assisted Drug Delivery. *Frontiers in Pharmacology* 2015, *6*, 1-13.

14) Malam, Y.; Loizidou, M.; Seifalian, A. Liposomes And Nanoparticles: Nanosized Vehicles For Drug Delivery In Cancer. *Trends in Pharmacological Sciences* 2009, *30*, 592-599.

15) Guo, P.; Yang, J.; Liu, D.; Huang, L.; Fell, G.; Huang, J.; Moses, M.; Auguste, D. Dual Complementary Liposomes Inhibit Triple-Negative Breast Tumor Progression And Metastasis. *Science Advances* 2019, *5*, eaav5010.

16) Faraday, M. Michael Faraday's recognition of ruby Au: the birth of modern nanotechnology. *Au Bulletin* **40**, 267-269 (2007).

17) Zsigmondy, R. & Norton, J. F. *The Chemistry of Col-loids.* John Wiley & Sons, Inc., New York, 1917

18) Svedberg, T. *The Formation of Colloids.* J. & A. Chu- rchill, London, 1921

19) Mishchenko, M.; Travis, L. Gustav Mie And The Evolving Discipline Of Electromagnetic Scattering By Particles. *Bulletin of the American Meteorological Society* 2008, *89*, 1853-1862.

20) Das, M.; Shim, K.; An, S.; Yi, D. Review On Gold Nanoparticles And Their Applications. *Toxicology and Environmental Health Sciences* 2011, *3*, 193-205.

21) An, L.; Wang, Y.; Lin, J.; Tian, Q.; Xie, Y.; Hu, J.; Yang, S. Macrophages-Mediated Delivery Of Small Gold Nanorods For Tumor Hypoxia Photoacoustic Imaging And Enhanced Photothermal Therapy. *ACS Applied Materials & Interfaces* 2019.

22) Zhang, F.; Han, X.; Hu, Y.; Wang, S.; Liu, S.; Pan, X.; Wang, H.; Ma, J.; Wang, W.; Li, S. et al. Interventional Photothermal Therapy Enhanced Brachytherapy: A New Strategy To Fight Deep Pancreatic Cancer. *Advanced Science* 2019, *6*, 1801507.

23) Gao, Y.; Chen, H.; Zhou, Y.; Wang, L.; Hou, Y.; Xia, X.; Ding, Y. Intraorgan Targeting Of Gold Conjugates For Precise Liver Cancer Treatment. *ACS Applied Materials & Interfaces*2017, *9*, 31458-31468.

24) Foulkes, R.; Ali Asgari, M.; Curtis, A.; Hoskins, C. Silver-Nanoparticle-Mediated Therapies In The Treatment Of Pancreatic Cancer. *ACS Applied Nano Materials* 2019, *2*, 1758-1772.

25) Ansari, S.; Ficiarà, E.; Ruffinatti, F.; Stura, I.; Argenziano, M.; Abollino, O.; Cavalli, R.; Guiot, C.; D'Agata, F. Magnetic Iron Oxide Nanoparticles: Synthesis, Characterization And Functionalization For Biomedical Applications In The Central Nervous System. *Materials* 2019, *12*, 465.

26) Zhang, H.; Liu, X.; Zhang, Y.; Gao, F.; Li, G.; He, Y.; Peng, M.; Fan, H. Magnetic Nanoparticles Based Cancer Therapy: Current Status And Applications. *Science China Life Sciences* 2018, *61*, 400-414.

27) Quan, Q.; Xie, J.; Gao, H.; Yang, M.; Zhang, F.; Liu, G.; Lin, X.; Wang, A.; Eden, H.; Lee, S. et al. HSA Coated Iron Oxide Nanoparticles As Drug Delivery Vehicles For Cancer Therapy. *Molecular Pharmaceutics* 2011, *8*, 1669-1676.

28) Kallu, J.; Banerjee, T.; Sulthana, S.; Darji, S.; Higginbotham, R.; Fletcher, C.; Gerasimchuk, N.; Santra, S. Nanomedicine-Assisted Combination Therapy Of NSCLC: New Platinum-Based Anticancer Drug Synergizes The Therapeutic Efficacy Of Ganetespib. *Nanotheranostics* 2019, *3*, 120-134.

29) Satpathy, M.; Wang, L.; Zielinski, R.; Qian, W.; Wang, Y.; Mohs, A.; Kairdolf, B.; Ji, X.; Capala, J.; Lipowska, M. et al. Targeted Drug Delivery And Image-Guided Therapy Of Heterogeneous Ovarian Cancer Using HER2-Targeted Theranostic Nanoparticles. *Theranostics* 2019, *9*, 778-795.

30) Torres Andón, F.; Alonso, M. Nanomedicine And Cancer Immunotherapy – Targeting Immunosuppressive Cells. *Journal of Drug Targeting* 2015, *23*, 656-671.

31) Couzin-Frankel, J. Cancer Immunotherapy. *Science* 2013, *342*, 1432-1433.

32) Chen, Q.; Xu, L.; Liang, C.; Wang, C.; Peng, R.; Liu, Z. Photothermal Therapy With Immune-Adjuvant Nanoparticles Together With Checkpoint Blockade For Effective Cancer Immunotherapy. *Nature Communications* 2016, *7*.

33) Jacobson, C.; Ritz, J. Time To Put The CAR-T Before The Horse. *Blood* 2011, *118*, 4761-4762.

34) Yang, Y. Cancer Immunotherapy: Harnessing The Immune System To Battle Cancer. *Journal of Clinical Investigation* 2015, *125*, 3335-3337.

35) C&EN 2018, 96, 19, 32-37

36) Dranoff, G. Cytokines In Cancer Pathogenesis And Cancer Therapy. *Nature Reviews Cancer* 2004, *4*, 11-22.

37) Lee, S.; Margolin, K. Cytokines In Cancer Immunotherapy. *Cancers* 2011, *3*, 3856-3893.

38) Acúrcio, R.; Scomparin, A.; Conniot, J.; Salvador, J.; Satchi-Fainaro, R.; Florindo, H.; Guedes, R. Structure–Function Analysis Of Immune Checkpoint Receptors To Guide Emerging Anticancer Immunotherapy. *Journal of Medicinal Chemistry* 2018, *61*, 10957-10975.

39) Mahoney, K.; Freeman, G.; McDermott, D. The Next Immune-Checkpoint Inhibitors: PD-1/PD-L1 Blockade In Melanoma. *Clinical Therapeutics* 2015, *37*, 764-782.

40) Sau, S.; Alsaab, H.; Bhise, K.; Alzhrani, R.; Nabil, G.; Iyer, A. Multifunctional Nanoparticles For Cancer Immunotherapy: A Groundbreaking Approach For

Reprogramming Malfunctioned Tumor Environment. *Journal of Controlled Release* 2018, *274*, 24-34.

41) Beatty, G.; Gladney, W. Immune Escape Mechanisms As A Guide For Cancer Immunotherapy. *Clinical Cancer Research* 2014, *21*, 687-692.

42) Santra, S.; Kaittanis, C.; Santiesteban, O.; Perez, J. Cell-Specific, Activatable, And Theranostic Prodrug For Dual-Targeted Cancer Imaging And Therapy. *Journal of the American Chemical Society* 2011, *133*, 16680-16688.

43) Thorn, C.; Oshiro, C.; Marsh, S.; Hernandez-Boussard, T.; McLeod, H.; Klein, T.; Altman, R. Doxorubicin Pathways. *Pharmacogenetics and Genomics* 2011, *21*, 440-446.

44) Santra, S.; Jativa, S.; Kaittanis, C.; Normand, G.; Grimm, J.; Perez, J. Gadolinium-Encapsulating Iron Oxide Nanoprobe As Activatable NMR/MRI Contrast Agent. *ACS Nano* 2012, *6*, 7281-7294.

45) O'Flynn, K.; Russul-Saib, M.; Ando, I.; Wallace, D. L., Beverley, P. C., Boylston, A. W., & Linch, D. C. Different pathways of human T-cell activation revealed by PHA-P and PHA-M. *Immunology*. 1986, 57(1), 55–60.

46) Deng, X.; Liu, J.; Wang, Y.; Wu, C; Jiang, J. Antitumor Mechanisms of Immune Checkpoints PD-L1/PD-1 Blockade in Cancer Treatment. *International Journal of Pharmaceutical Science Invention* 2014, *3*, 12, 31-38.